



HAL
open science

Stochastic Bayesian inversion of borehole self-potential measurements

W. F. Woodruff, A. Revil, Abderrahim Jardani, D. Nummedal, S. Cumella

► **To cite this version:**

W. F. Woodruff, A. Revil, Abderrahim Jardani, D. Nummedal, S. Cumella. Stochastic Bayesian inversion of borehole self-potential measurements. *Geophysical Journal International*, 2010, 183 (2), pp.748-764. 10.1111/J.1365-246X.2010.04770.X . insu-00565381

HAL Id: insu-00565381

<https://insu.hal.science/insu-00565381>

Submitted on 11 Mar 2021

HAL is a multi-disciplinary open access archive for the deposit and dissemination of scientific research documents, whether they are published or not. The documents may come from teaching and research institutions in France or abroad, or from public or private research centers.

L'archive ouverte pluridisciplinaire **HAL**, est destinée au dépôt et à la diffusion de documents scientifiques de niveau recherche, publiés ou non, émanant des établissements d'enseignement et de recherche français ou étrangers, des laboratoires publics ou privés.

Stochastic Bayesian inversion of borehole self-potential measurements

W. F. Woodruff,¹ A. Revil,^{1,2} A. Jardani,³ D. Nummedal⁴ and S. Cumella⁵

¹Colorado School of Mines, Department of Geophysics, Green Center, 1500 Illinois street, 80401 Golden, CO, USA. E-mail: arevil@mines.edu

²LGIT, UMR 5559, CNRS, Equipe Volcan, Université de Savoie, 73376 Le Bourget-du-lac Cedex, France

³UMR 6143 CNRS, Université de Rouen Bât. IRESE A, 76821 Mont-Saint-Aignan Cedex, France

⁴Colorado School of Mines, CERL, 1500 Illinois Street, Golden, CO 80401, USA

⁵Bill Barrett Corp., 1099 18th Street Ste. 2300, Denver, CO 80202, USA

Accepted 2010 August 9. Received 2010 July 11; in original form 2009 December 24

SUMMARY

We propose a mechanistic model to compute and to invert self-potential log data in sedimentary basins and for near-surface geophysical applications. The framework of our analysis is founded in a unified electrical conductivity and self-potential petrophysical model. This model is based on an explicit dependence of these properties on porosity, water saturation, temperature, brine salinity, cementation and saturation (Archie) exponents and the volumetric charge density per unit pore volume associated with the clay fraction. This model is consistent with empirical laws widely used to interpret self-potential logs according to the two limiting cases corresponding to a clean sand and a pure shale. We present a finite element calculation of the self-potential signal produced by sand reservoirs interstratified with shale layers. For layered strata normal to the well, we demonstrate that the 3-D Poisson equation governing the occurrence of self-potentials in a borehole can be simplified to a 2-D axisymmetric partial differential equation solved at each depth providing a common self-potential reference can be defined between these different depths. This simplification is very accurate as long as the vertical salinity gradients are not too strong over distances corresponding to the borehole diameter. The inversion of borehole data (self-potential, resistivity and density well logs, incorporating information derived from neutron porosity and gamma-ray log data) is performed with the Adaptive Metropolis Algorithm (AMA). We start by formulating an approximate analytical solution for the six model parameters (water saturation, porosity, the two Archie's exponents, the pore water conductivity and the volumetric charge density of the diffuse layer). This solution is used for the AMA algorithm to converge in less than 60 iterations at each depth for the real case study. The posterior probability distributions are computed using 50–60 additional realizations. Our approach is applied to a case study concerning a small sedimentary sequence in the Piceance Basin, Colorado, in a series of tight gas reservoirs.

Key words: Electrical properties; Electromagnetic theory; Hydrogeophysics; Permeability and porosity.

1 INTRODUCTION

Self-potential signals are passively recorded electrical potentials at the surface of the Earth or in boreholes. They evidence underlying non-equilibrium physical and chemical processes occurring naturally in the conductive ground. Common examples include the flow of the ground water (Sill 1983) or the existence of gradients in the activity of ionic species and redox potentials (Maineult *et al.* 2005, 2006; Arora *et al.* 2007; Minsley *et al.* 2007a,b; Mendonça 2008; Revil *et al.* 2009). The development of the self-potential method as a quantitative tool is fairly recent in hydrogeophysics. For instance, this method has been used to reconstruct the shape of the water table

and to determine permeability and storativity for ground water flow problems (Jardani *et al.* 2007, 2008, 2009; Minsley *et al.* 2007a), to determine the distribution of the redox potential in contaminant plumes (Linde & Revil 2007; Minsley *et al.* 2007b) and to locate ore bodies in mineral exploration (Mendonça 2008). A general mechanistic theory for self-potential signals in porous media has been developed recently by Revil & Linde (2006) and Revil (2007). Complementary investigations for the redox component can be found in Arora *et al.* (2007) for contaminant plumes and in Castermant *et al.* (2008) for the corrosion of ore bodies or metallic pipes.

Self-potential wireline surveys are among the oldest geophysical methods and are still commonly performed nowadays to

characterize oil and gas reservoirs. In addition, the development of new logging tools with multisensors including self-potential (e.g. Winter *et al.* 1991; Pezard *et al.* 2009) motivate the development of new analysis of borehole measurements. Indeed the challenge underlined by the inversion of self-potential data in boreholes, jointly to complementary measurements, is motivated not just by the interpretation of several logs together but also by the use of these new type of logging tools for shallow uncased boreholes filled with water. In deeper boreholes drilled by the oil industry, downhole self-potential measurements comprising regularly spaced *in situ* measurements of the electrical potential in the borehole environment (filled with mud) using a pair of electrodes (e.g. Worthington & Meldau 1958; Segesman 1962). Historically, self-potential log data have been used in conjunction with resistivity log data to determine the salinity of connate (pore) water and cementation exponent (Salazar *et al.* 2008). Borehole self-potential measurements have also been used as a qualitative indicator of permeability associated with fractures (Hötzl & Merkle 1989; Hunt & Worthington 2000), a shale marker for stratigraphic correlation purposes and to determine the formation thickness or dip angle (Doll 1949; Pirson 1963). Stoll *et al.* (1995) have used the *in situ* measurement of self-potentials to determine the redox component of the self-potential anomaly associated with the presence of graphite in a fault plane.

Despite the simplicity of the method, the treatment and analysis of self-potential data is largely empirical in the literature. Relatively few papers have provided a quantitative approach to interpret self-potential signals in boreholes. Even in recent works (Zhang & Wang 1999; Salazar *et al.* 2008; Pan *et al.* 2009), the so-called static spontaneous potential (SSP) approximation (described in detail below) remains the basis for self-potential data analysis in sedimentary basins.

We present below a quantitative theory of self-potential signals recorded in boreholes drilled in sedimentary basins. Relevant applications for the theory include the analysis and interpretation of self-potential signals in oil and gas reservoirs and the estimation of petrophysical properties of clay-rock formations potentially suited for long-term storage of nuclear wastes. In general, this theory can be implemented in any problem related to the characterization of *in situ* properties of geological systems including in the shallow subsurface. The general theory is described in details in Section 2. In Section 3, we provide details on a methodology for forward and stochastic inverse modelling of borehole measurements including self-potential data. A synthetic case is discussed in Section 4 to benchmark a simplified 2-D axisymmetric model and prove that our algorithm converges to the true solution. The inversion algorithm and an application to a case study are described in Section 5.

2 THEORY

2.1 Principle

Self-potential signals result from a difference of electrical potential between a reference electrode and a moving electrode without the injection of electrical current. The reference electrode is located close to the borehole, at the ground surface. The moving electrode traverses the subsurface in an uncased borehole and is in electrical contact with the formation through the mud filling the borehole for oil industry-related applications and through water for near-surface geophysical applications. Measurements are recorded as a difference of electrical potential between the two electrodes at regular depth intervals using a DC-voltmeter with a high input

impedance (typically >10 Mohm) and a high resolution (at least 0.1 mV). Repeatability of the measurements is usually 2 mV in baseline shift (Ellis & Singer 2007).

2.2 Underlying theory

The self-potential log is usually governed by the difference in the electrochemical potential of the charge carriers (ions in the present case) between the formation and the drilling fluid. In addition, a streaming potential component can occur if the drilling fluid infiltrates the formations or if the formation water flows into the borehole (Hearst & Nelson 1985; Taherian *et al.* 1995). In boreholes drilled by the oil industry, the mud pressure is adjusted to compensate for the fluid over- or underpressures with respect to hydrostatic.

In a porous material saturated by brine, the total electrical current density \mathbf{j} (in A m^{-2}) is given by (Sill 1983; Jardani *et al.* 2007, 2008, 2009; Minsley *et al.* 2007a,b and references therein),

$$\mathbf{j} = \sigma_0 \mathbf{E} + \mathbf{j}_s, \quad (1)$$

where \mathbf{E} is the electrical field (in V m^{-1} ; in the quasistatic limit of the Maxwell equations $\mathbf{E} = -\nabla\psi$, where ψ is the electrical potential expressed in V), σ_0 is the DC-electrical conductivity of the porous material (in S m^{-1}) and \mathbf{j}_s is a source current density (in A m^{-2}) associated with any potential disturbance that can affect the movement of charge carriers. Eq. (1) stands for a generalized Ohm's law and the first term on the right-hand-side of eq. (1) corresponds to the classical conduction term (classical Ohm's law). In addition to the previous constitutive equation, we need a continuity equation to determine a field equation for the electrostatic potential ψ . The continuity equation for the conservation of the electrical charge, in the low-frequency limit of the Maxwell equations, is $\nabla \cdot \mathbf{j} = 0$ (the total current density is conservative).

Revil & Linde (2006) have built a model to capture both the effect of porosity and the multicomponent ionic characteristics of the electrolyte upon the source current density. For a brine-saturated porous material, the total source current density is given by (Revil & Linde 2006, eq. 182),

$$\mathbf{j}_s = \bar{Q}_V \mathbf{u} - k_b T \sum_{i=1}^N \frac{T_i \sigma_0}{q_i} \nabla \ln\{i\}, \quad (2)$$

where k_b is the Boltzmann constant ($1.381 \times 10^{-23} \text{JK}^{-1}$), $\{i\}$ is the activity of species i (taken equal to the concentration of species i for an ideal solution), \bar{Q}_V is the volumetric (moveable) charge per unit pore volume at saturation (expressed in C m^{-3} and related to the electrical diffuse layer), \mathbf{u} represents the Darcy velocity (in m s^{-1}), q_i is the charge of species i dissolved in water (in C) and T_i (dimensionless) is the macroscopic Hittorf number of the ionic species i in the porous material (i.e. the fraction of electrical current carried by this species). Eq. (2) can be easily generalized for unsaturated materials yielding,

$$\mathbf{j}_s = \frac{\bar{Q}_V}{s_w} \mathbf{u} - k_b T \sum_{i=1}^N \frac{T_i(s_w) \sigma_0(s_w)}{q_i} \nabla \ln\{i\}, \quad (3)$$

where $0 \leq s_w \leq 1$ represent the (relative) water saturation (see Linde *et al.* 2007 and Revil *et al.* 2007 for the electrokinetic component and Revil 1999 and Revil *et al.* 2009, for the electrochemical component).

In the following, we assume that the pore water can be treated as a binary symmetric 1:1 electrolyte like NaCl, to simplify the presentation, although keeping in mind that using true pore water

composition (through *in situ* sampling) is still a possible choice. Several models have been developed to describe the conductivity and diffusion potential responses of porous media (see Revil *et al.* 1998; Revil 1999 and references therein), according to which electrical conductivity has two contributions: a contribution coming from electrical conduction through the bulk pore water and a surface contribution from the electrical double layer coating the hydrated mineral surface (Bolève *et al.* 2007; Mojid & Cho 2008; Ugbo *et al.* 2009). In the following, for its simplicity and robustness, we use the classical Waxman & Smits (1968) model to interpret log data; however, other models based on the differential effective medium approach could represent alternative options (see Revil *et al.* 1998 and Gelius & Wang, 2008 and references therein). The Waxman & Smits (1968) model yields,

$$\sigma_0 = \sigma_{(+)} + \sigma_{(-)}, \quad (4)$$

$$\sigma_{(+)} = \frac{s_w^n}{F} \left(t_{(+)} \sigma_w + \frac{\beta_S Q_V}{s_w} \right), \quad (5)$$

$$\sigma_{(-)} = s_w^n (1 - t_{(+)}) \frac{\sigma_w}{F}, \quad (6)$$

$$T_{(\pm)} = \frac{\sigma_{(\pm)}}{\sigma_0}, \quad (7)$$

$$Q_V = \tilde{\rho}_S \left(\frac{1 - \phi}{\phi} \right) \text{CEC}, \quad (8)$$

where $\sigma_{(\pm)}$ are the contributions of cations (+) and anions (−) to the overall rock conductivity, σ_w is the brine conductivity (S m^{-1}), $\beta_S = (1 - f)\beta_{(+)}$ is the effective cation mobility along the mineral surface, $\beta_{(+)}$ is the mobility of the cations in the pore water ($\text{m}^2 \text{s}^{-1} \text{V}^{-1}$), $\tilde{\rho}_S$ is the mass density of the solid phase, f is the fraction of counterions in the Stern layer (typically equal to 0.98 for kaolinite, 0.85 for illite and 0.90 for smectite, see Leroy *et al.* 2007), CEC is the cation exchange capacity of the clay fraction, F is the electrical formation factor (dimensionless) given by Archie's law, $F = \phi^{-m}$ (Archie 1942), m is called the cementation exponent (Archie's first exponent), s_w is the relative saturation of the water phase, n is the saturation exponent (Archie's second exponent) and $t_{(+)}$ is the microscopic Hittorf number of the cations in the brine (Revil 1999). This microscopic Hittorf number is defined by,

$$t_{(+)} = \frac{\beta_{(+)}}{\beta_{(+)} + \beta_{(-)}}, \quad (9)$$

where $\beta_{(-)}$ is the mobility of the anions in the pore water. In the absence of surface conductivity, the macroscopic Hittorf numbers of the material $T_{(\pm)}$ are equal to the microscopic Hittorf numbers $t_{(\pm)}$. Pore water conductivity is related to the mobility of the ions $\beta_{(\pm)}$ by,

$$\sigma_w = e C_w (\beta_{(+)} + \beta_{(-)}), \quad (10)$$

where C_w is the salinity of the pore water (usually reported in Mol L^{-1} but is expressed in m^{-3} in SI units). The temperature dependence of ionic mobility is given by (Revil *et al.* 1998),

$$\beta_{(\pm)}(T) = \beta_{(\pm)}(T_0) [1 + \alpha_w (T - T_0)], \quad (11)$$

where $\alpha_w = 0.023$ per $^\circ\text{C}$. This relationship governs both the temperature dependence of the connate water and surface conductivities.

The volumetric charge density of the electrical diffuse layer \bar{Q}_V is related to the total volumetric charge density by,

$$\bar{Q}_V = (1 - f) Q_V. \quad (12)$$

The partition coefficient f of the counterions can be determined from electrical triple layer models (see Leroy *et al.* 2007, 2008; Jougnot *et al.* 2009).

Revil (1999) showed the gradient of the logarithm of the activity of the salt is equivalent to the gradient of the logarithm of the conductivity of the salt. Using this change of variable, we can rewrite the total source current as,

$$\mathbf{j}_S = \frac{\bar{Q}_V}{s_w} \mathbf{u} - \frac{k_b T}{e} \sigma_0 (2T_{(+)} - 1) \nabla \ln \sigma_w. \quad (13)$$

Combining eq. (1) with the continuity equation for the charge $\nabla \cdot \mathbf{j} = 0$, the self-potential field ψ in a borehole is the solution to the following Poisson equation,

$$\nabla \cdot (\sigma \nabla \psi) = \nabla \cdot \mathbf{j}_S, \quad (14)$$

where the volumetric source current density $\mathfrak{S} = \nabla \cdot \mathbf{j}_S$ (in A m^{-3}) is computed using eq. (13). Eqs (13) and (14) are the two fundamental equations governing the occurrence of self-potential signals in boreholes. In the following, we solve eq. (14) using a finite element code. It can be solved in 3-D, as the complete solution to eq. (14) or at each depth (1-D axisymmetric approximation) assuming in 2-D layered formations normal to the well, or at each depth (2-D axisymmetric approximation) assuming the (vertical) self-potential contribution produced at the interfaces between geological layers can be neglected with respect to the (radial) contributions arising between the formations and the borehole. This last assumption will be tested later in the paper and shown to be an excellent approximation for our analysis as long as the vertical gradient in connate water salinity is not too severe. Fig. 1(a) shows where the current sources can be located at the interface between the borehole and the formations and between the invaded zone (filled with the mud filtrate) and the uninvaded zone and between the invaded zone and the shale layers.

2.3 Temperature correction

A temperature correction must be applied before borehole self-potential measurements can be analysed quantitatively. Indeed, due to the geothermal gradient along the borehole, the reference and moving electrodes are typically at different temperatures. Because the electrode response is intrinsically temperature dependent (Petiau 2000), a differential of electrical potential develops between the two electrodes, even in the absence of any external source of electrical current. As a result, the self-potential log drifts with depth, as a function of the corresponding increase in formation temperature. A straightforward correction can be used to remove this dependence from the data. A first-order Taylor expansion of the electrical potential, measured by the moving electrode, with respect to temperature is,

$$\psi(T) = \psi(T_0) + \psi'(T_0)(T - T_0) + \text{O}(T^2), \quad (15)$$

where $\psi'(T_0)$ is the first derivative of $\psi(T)$ with respect to temperature. Eq. (1) is therefore just a linear approximation of the temperature in the vicinity of T_0 . If we assume that T_0 is the temperature of the reference electrode and T is the temperature at position z of the moving electrode, the difference of electrical potential between the moving electrode and the reference electrode (assumed to be identical) is,

$$\delta\psi = \psi(T) - \psi(T_0) = \alpha(T - T_0), \quad (16)$$

where $\alpha = \psi'(T_0)$. The temperature coefficient α depends on the type of electrode used. Lead, bronze and stainless electrodes are

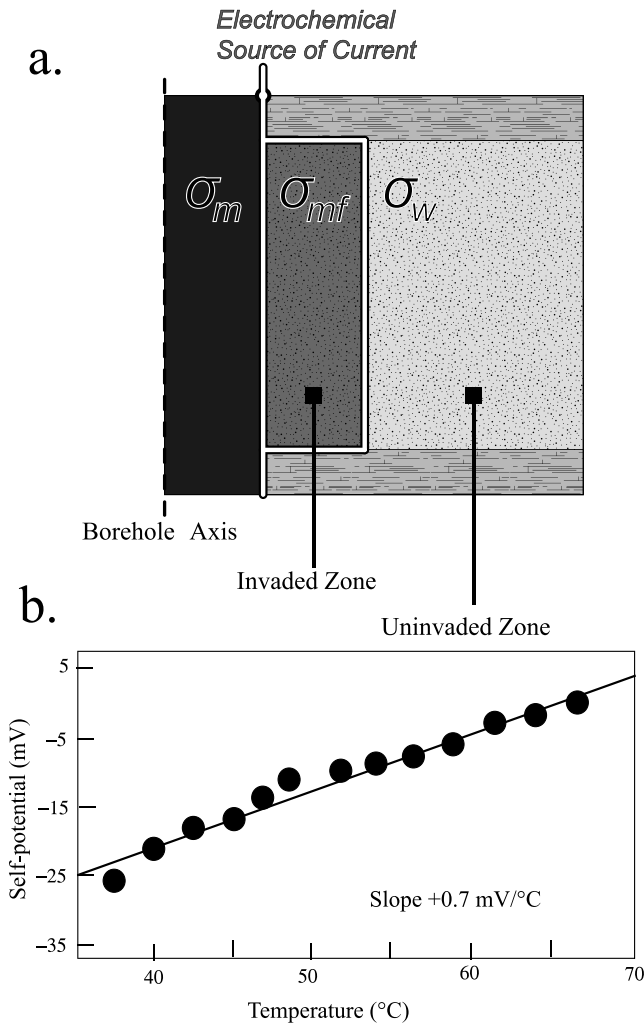


Figure 1. Self-potential borehole measurements. (a) The self-potential current sources are mainly located at interface where there is a steep gradient in the chemical potential of the brine, therefore at the interface between the borehole and the formation and at the interface between the invaded and uninvasion zones. Here the mud infiltrates invades a sand layer sandwiched between two shale layers (σ_m represents the conductivity of the mud, σ_{mf} represents the conductivity of the mud filtrate inside the pore of the sand in the invaded zone and σ_w represents the conductivity of the pore water in the invaded part of the sand formation). (b) Self-potential data versus *in situ* temperature in a relatively homogeneous section of a borehole drilled in the Piceance Basin, Colorado. Each point represents an average over a depth interval. This trend ($\sim 0.7 \text{ mV}^\circ\text{C}^{-1}$) corresponds to the known dependence of Cu/CuSO₄ electrodes. The slope is used to correct the ‘drift’ common to self-potential borehole data.

often used for the moving electrode. For these electrode types, the temperature coefficient α can be determined from the Nernst equation. In the case of non-polarizing electrodes, α can be determined experimentally (see Table 1 for some values). This coefficient can be either positive or negative. If the type of electrode used to make the measurements is unknown, as in the case analysed later in this paper, the temperature coefficient can be determined by an empirical first-order fit of the self-potential data versus temperature as shown in Fig. 1(b).

After the temperature correction has been applied, the data must be shifted to a common reference. The classical approach, widely used in industry, incorporates a bulk shift of the data to the shale baseline, which is picked empirically for each well. Although it

Table 1. Typical temperature dependence of some electrodes.

Electrode	Temperature coefficient at around 25°C
Pb/PbCl ₂	0.20 mV/°C ^a
Cu/CuSO ₄	0.7 mV/°C ^b , 0.9 mV/°C ^c
Ag/AgCl	-0.43 mV/°C ^d , -0.73 mV/°C ^e

^aPetiau (2000)

^bSaturated copper sulfate, Antelman (1989)

^cClennel Palmer & King (2004)

^d0.1 N KCl, Antelman (1989)

^e3.5 M KCl solutions, $0 < T < 100^\circ\text{C}$ (Rieger 1994)

allows for comparison of the data across a multiwell data set, this process is entirely qualitative and can eliminate characteristic aspects of the self-potential curve. Due to the inherent subjectivity of this method, as well as the detrimental effect on the data, we undertake an alternative approach. In our treatment of the self-potential log, the temperature corrected data is shifted to a common reference potential (zero reference). Due to the relative nature of the measured electrical potential to a reference voltage, a number of methods can be used to obtain a valid reference. In this work, the reference potential is determined theoretically from the data. A detailed description of the approach we use to define the reference potential is given in Appendix A. Zero referencing the self-potential log has the advantages of preserving the raw data, while normalizing the data set, which is useful for both correlation and modelling purposes.

2.4 Comparison with the empirical approach

In the present section, we demonstrate our formulation is consistent with simplified formulae widely used to determine the formation water resistivity from the self-potential log. Neglecting the streaming potential contribution (i.e. imposing the condition that the borehole and the formation are at the same fluid pressure) and using the equilibrium condition $\mathbf{j} = 0$ in eqs (1) and (13) (i.e. the diffusion current is exactly counterbalanced by the conduction current), we obtain,

$$\frac{k_b T}{e} (2T_{(+)} - 1) \nabla \ln \sigma_w + \nabla \psi = 0. \quad (17)$$

The difference of electrical potential between the formation water and the fluid filling the borehole is therefore obtained from eq. (17),

$$\Delta \psi = -\frac{k_b T}{e} (2T_{(+)} - 1) \ln \left(\frac{\sigma_m}{\sigma_w} \right). \quad (18)$$

To compare this formula with a classical formula found in the literature, we denote $\rho_m = 1/\sigma_m$ as the electrical resistivity of the drilling mud (or borehole fluid) and $\rho_w = 1/\sigma_w$ as the resistivity of the pore water.

For the end-member case of a pure diffusion potential corresponding to a clean sand, surface conductivity can be neglected and using $\bar{Q}_V = 0$ in eq. (7) to (9), we obtain $T_{(+)} = t_{(+)}$. Therefore the sand self-potential baseline is given by equating $T_{(+)} = t_{(+)}$ in eq. (18). This yields,

$$\Delta \psi_{sd} = \frac{k_b T}{e} (2t_{(+)} - 1) \ln \left(\frac{\rho_m}{\rho_w} \right), \quad (19)$$

where $k_b T/e = 25.8 \text{ mV}$ at 25°C. The reciprocal end-member case corresponds to a perfect membrane also called the shale baseline in the literature (Ellis & Singer 2007). In this case, surface conductivity dominates and $T_{(+)} = 1$ (all the current is carried by the cations as a result of the strong effect of surface conductivity in the electrical

double layer). Considering $T_{(+)} = 1$ eq. (18) yields the following expression for the shale baseline,

$$\Delta\psi_{sh} = \frac{k_b T}{e} \ln\left(\frac{\rho_m}{\rho_w}\right). \quad (20)$$

This electrical potential response is also called the perfect membrane potential. Eqs (19) and (20) do not contain any material properties, therefore they are model independent. They are, however, dependent on the conductivity, or resistivity, of the pore water. Consequently, they have been widely used in the literature to determine the formation water salinity (e.g. Ellis & Singer 2007 and references therein).

The so-called SSP is the ideal self-potential curve produced by the transition from shale to a thick, porous, clean sand (Ellis & Singer 2007). Using $\ln x = 2.303 \log x$, the above definition and Eqs (19) and (20), the SSP is given by,

$$SSP = -K \log\left(\frac{\rho_m}{\rho_w}\right), \quad (21)$$

$$K = \frac{4.606 k_b T}{e} (1 - t_{(+)}), \quad (22)$$

which yields $K = 72$ mV at 25°C and $K = 103$ mV at 150°C using $t_{(+)} = 0.39$, the microscopic Hittorf number for a sodium chloride solution (see Revil 1999). This is consistent with the formula found in the literature where $K = 65 + 0.24 T$ where T is expressed in $^\circ\text{C}$ ($K = 71$ mV at 25°C and $K = 101$ mV at 25°C) (see Ellis & Singer 2007). Usually eq. (21) has to be corrected for the borehole diameter given by the caliper log (Tabanou *et al.* 1987).

Salazar *et al.* (2008) proposed a model based on the equations developed by Zhang & Wang (1997, 1999). Their model is equivalent to a dipole layer of electrical charges with a potential difference across the dipole layers given by the SSP model. As discussed above this approach oversimplifies the physics of the problem because the SSP model works only if both the clean sand and shale baselines are both present and contiguous within the formation. Essentially, the ideal SSP case misrepresents the true nature of the self-potential response in the borehole environment. Many researchers still consider the self-potential response in a borehole is due to a potential generator at the interface between the formations and the borehole. Although these boundaries may, in fact, coincide spatially with an actual current source, the concept is unphysical. Hence this traditional view should be deprecated, since self-potential signals are always generated by a source of current, as evidenced by the governing Poisson equation, eq. (14). We propose a more general theory, in which the macroscopic Hittorf number $T_{(+)}$ may take any value between 1 (i.e. the shale baseline or the case for membrane potential) and $t_{(+)}$ (i.e. the clean sand baseline or the case for pure diffusion potential), which accounts for contributions from both positively and negatively charged ionic species, as well as the contributions from surface conductance. In the following section, we will develop a method to invert *in situ* self-potential measurements in terms of formation and reservoir properties.

3 FORWARD AND INVERSE MODELLING

3.1 Forward finite element modelling

Eq. (14) is solved to provide the distribution of self-potential ψ using eq. (13) to determine the volumetric source current density $\mathfrak{S} = \nabla \cdot \mathbf{j}_s$. Eq. (14) can be solved with any type of numerical partial

differential equation solver. In this work, we use the finite element software Comsol Multiphysics 3.5 to solve the forward problem numerically with appropriate boundary conditions for which the normal component of the electrical field is either null at interfaces with an insulating boundary or electrically grounded from the current sources located at the interface between the well and the formation. Jardani *et al.* (2007, 2008, 2009) described various examples of solving the self-potential problem with Comsol Multiphysics and the boundary conditions to be used.

If we consider a layered system in which the geological layers are normal to the well, the volumetric (i.e. 3-D) solution to the Poisson eq. (14) is solved using a 2-D axisymmetric space parametrized in terms of z , the vertical component (assuming a vertical well) and r , the radial component. We will call this model the 2-D axisymmetric model below. We will show, to a good approximation, the resolution of eq. (14) can be reduced to a series of 2-D problems solved independently at each depth using only the dependence of the source current density on radial distance from the borehole axis (named the 1-D axisymmetric model hereinafter). This ‘simplified’ model neglects the vertical potential contribution to the self-potential signals; however, it has many advantages over the general model due to the fact it can be parallelized, thereby decreasing computational cost and can be applied iteratively to a data set of arbitrary size.

Regarding the boundary condition, we use a Dirichlet condition far from the well. Rejecting the Dirichlet condition far from the source does not improve the accuracy of the modelling of the potential within the medium. This is because the further the boundary, the bigger the surface on which this condition is given, increasing its influence. A zero Dirichlet condition makes the potential in a midpoint of the source and that boundary be more or less half of the correct value. The real improvement in putting the Dirichlet condition far from the source is to improve the potential accuracy in the vicinity of the source itself that is in a domain small with respect to the distance from the source to the external boundary. Our approach is therefore correct only because we stay in the vicinity of the source, that is we measure the potential inside the borehole with a source of current mainly located at the borehole/sediment interface.

3.2 Starting value of the model parameter vector

We propose an algorithm to invert the following six petrophysical formation properties: the pore water conductivity (alternatively, connate water salinity), the formation factor (alternatively, the porosity), the water saturation, the volumetric excess charge density (alternatively, the cation exchange capacity) and the two Archie exponents m and n using a joint inversion of various downhole measurements including resistivity, self-potential, density, neutron and gamma-ray logs. In this section, we use first-order approximations to determine a starting set of values for the previously mentioned model parameters to initiate the Markov Chain Monte Carlo (MCMC) algorithm.

The prior value for the porosity is usually determined as the average of the porosity estimate obtained from the density log and neutron porosity logs,

$$\phi = \frac{1}{2} (\phi_D + \phi_N), \quad (23)$$

$$\phi_D = \frac{\tilde{\rho} - \tilde{\rho}_S}{\tilde{\rho}_w - \tilde{\rho}_S}, \quad (24)$$

which is valid throughout regions of uniform borehole diameter

defined by the caliper log. In the following, we use $\tilde{\rho}_S = 2650 \text{ kg m}^{-3}$ (the mass density of silica) as a reasonable value for the mass density of the solid phase (Revil & Leroy 2001). However, if the borehole diameter is greater than approximately 10 per cent of the average diameter over a discrete interval measuring less than the length of the logging tool ($< \sim 10 \text{ m}$), which occurs frequently in shale intervals due to washout (i.e. increased erosion) of the borehole walls, the density curve exhibits anomalously low readings. This artefact of the density measurement results from the presence of a fluid-filled void between the logging tool and the formation when the sonde is flush with the, otherwise relatively smooth, borehole wall. The data over washed-out intervals are discarded and replaced with an interpolated linear approximation.

The apparent resistivity, ρ_a (in Ohm m) can be determined from a linear relationship between the resistivity of the invaded zone, ρ_{XO} (in Ohm m) and the true formation resistivity, ρ_f (in Ohm m) (Ellis & Singer 2007),

$$\rho_a = J(d_i)\rho_{XO} + [1 - J(d_i)]\rho_f, \quad (25)$$

$$\rho_{XO} = F\rho_{mf}, \quad (26)$$

where ρ_{mf} is the resistivity of the mud filtrate (in Ohm m) and $J(d_i)$ is a dimensionless constant that depends on d_i , the diameter of the invaded zone comprising the borehole diameter plus the depth of invasion. For our problem, the borehole diameter is $\sim 0.2032 \text{ m}$ (8 inches). According to the charts presented by Ellis & Singer (2007, p. 109), an appropriate value of $J(d_i)$ is 0.03. Eq. (25) is used to compute the formation resistivity using the apparent resistivity from deep induction measurements and the caliper log.

For a formation containing fluid phases of water and gas, the density log provides a measurement of the mass density of the formation $\tilde{\rho}$, which is related in turn to the porosity ϕ and the relative water saturation s_w by,

$$\tilde{\rho} = (1 - \phi)\tilde{\rho}_S + \phi s_w \tilde{\rho}_w + \phi(1 - s_w)\tilde{\rho}_g, \quad (27)$$

where $\tilde{\rho}_S$ and $\tilde{\rho}_g$ are the mean value of the mass density of the solid phase and the gas phase, respectively. Because the density of the gas is very low, the last term of eq. (27) is neglected. A first estimate of the relative water saturation is therefore given by,

$$s_w^1 = \begin{cases} \frac{\tilde{\rho} - (1 - \phi)\tilde{\rho}_S}{\phi\tilde{\rho}_w} & \text{if } \frac{\tilde{\rho} - (1 - \phi)\tilde{\rho}_S}{\phi\tilde{\rho}_w} \leq 1 \\ 1 & \text{if } \frac{\tilde{\rho} - (1 - \phi)\tilde{\rho}_S}{\phi\tilde{\rho}_w} > 1 \end{cases}. \quad (28)$$

Assuming the starting values for m and n (the two Archie exponents) equal 2, the electrical conductivity is taken from Eqs (4) to (8) by the following expression,

$$\sigma_0 = s_w^2 \phi^2 \sigma_w + \beta_S s_w \phi^2 Q_V, \quad (29)$$

which is a quadratic equation with respect to s_w . If we have an estimation of the conductivity of the pore water, either from eq. (21) or from *in situ* sampling, we can use eq. (29) to estimate a starting value for the charge density per unit pore volume according to,

$$Q_V = \frac{1/\rho_f - s_w^2 \phi^2 \sigma_w}{\beta_S s_w \phi^2}, \quad (30)$$

where $\rho_f = 1/\sigma_0$ is the formation resistivity determined from deep induction data for instance. In eq. (30), the porosity is determined from eq. (23). The cation exchange capacity is related to the CEC of the clay fraction, denoted CEC_{clay} and the gamma-ray (in API units) as (e.g. Rabaute *et al.* 2003),

$$\text{CEC} = I_{GR} \text{CEC}_{\text{clay}}, \quad (31)$$

$$I_{GR} = \frac{GR - GR_{Min}}{GR_{Max} - GR_{Min}}, \quad (32)$$

where I_{GR} is called the gamma-ray index. In the following, we use $GR_{Min} = 10$ for sand. These equations assume radioactive minerals, potassium for instance, are carried by the clay fraction. However, this assumption can be invalid where radioactive feldspar is present, in which case, sand formations are radioactive and could be misinterpreted as clay-rich formations. For the present case, the assumption of non-feldspathic (i.e. potassium free) sands is reasonable; thus, the total charge per unit volume is given by,

$$Q_V = \tilde{\rho}_S \frac{1 - \phi}{\phi} I_{GR} \text{CEC}_{\text{clay}}. \quad (33)$$

Combining Eqs (30) and (33), we obtain the following equation for the cation exchange capacity of the clay fraction,

$$\text{CEC}_{\text{clay}} = \frac{\phi}{\tilde{\rho}_S(1 - \phi)I_{GR}} \left(\frac{1/\rho_f - s_w^2 \phi^2 \sigma_w}{\beta_S s_w \phi^2} \right), \quad (34)$$

A second estimate of the connate fluid saturation is given by solving eq. (29) for the saturation term,

$$s_w^2 = -\frac{\beta_S Q_V \phi^2 - \sqrt{(\beta_S Q_V \phi^2)^2 + 4\sigma_w \phi^2}}{2\phi^2 \sigma_w}. \quad (35)$$

Hence, we have derived two equations for the determination of a prior value, at each depth, for the saturation of connate (pore) water. They are given by eqs (28) and (35). A relation of the density and neutron curves generates one curve, whereas the gamma-ray and deep resistivity curves are used to generate the second curve. Hence, the prior value for water saturation at each depth is given by a simple arithmetic average of these two estimates,

$$s_w = \frac{1}{2} (s_w^1 + s_w^2). \quad (36)$$

In the absence of the ideal case for which a value of the SSP response can be accurately calculated, a first estimation of the pore water conductivity σ_w can be obtained by solving eq. (29) with the porosity and deep resistivity logs in conjunction with fluid saturations obtained from either or both of the methods described above. A flowchart summarizing the formulation of the first estimation of the solution is given in Fig. 2.

The concentration of dissolved ions in water is directly related to fluid conductivity, or resistivity. The resistivity is measured as 2.0 Ohm m for the drilling mud, 1.5 Ohm m for the mud filtrate and a prior value of 0.5 Ohm m is assumed for the pore water. Corresponding salinities in Mol m^{-3} are calculated using eq. (10).

3.3 Development of a stochastic approach

We adopt a Bayesian approach to estimate posterior probability densities of the six material properties $\mathbf{m} = [\log \rho_w, \log Q_V, \text{logit } \phi, \text{logit } s_w, \log(m - 1), \log(n - 1)]$ from four downhole measurements: the gamma-ray, electrical resistivity, density and self-potential logs. We use the logarithm of the different material properties m_0 to ensure the positiveness of the random model parameters, the logit transform $\text{logit}(a) = \log[a/(1 - a)]$ when the parameter 'a' is a concentration greater than zero and less than one, $0 \leq a \leq 1$ (see Ghorbani *et al.* 2007). The previous choice is used to naturally impose the following constraints during the inversion $\rho_w > 1$, $Q_V > 0$, $0 < \phi < 1$, $0 < s_w < 1$, $m, n > 1$.

The Bayesian solution to the inverse problem presented here is based on the precept of combining information from borehole data

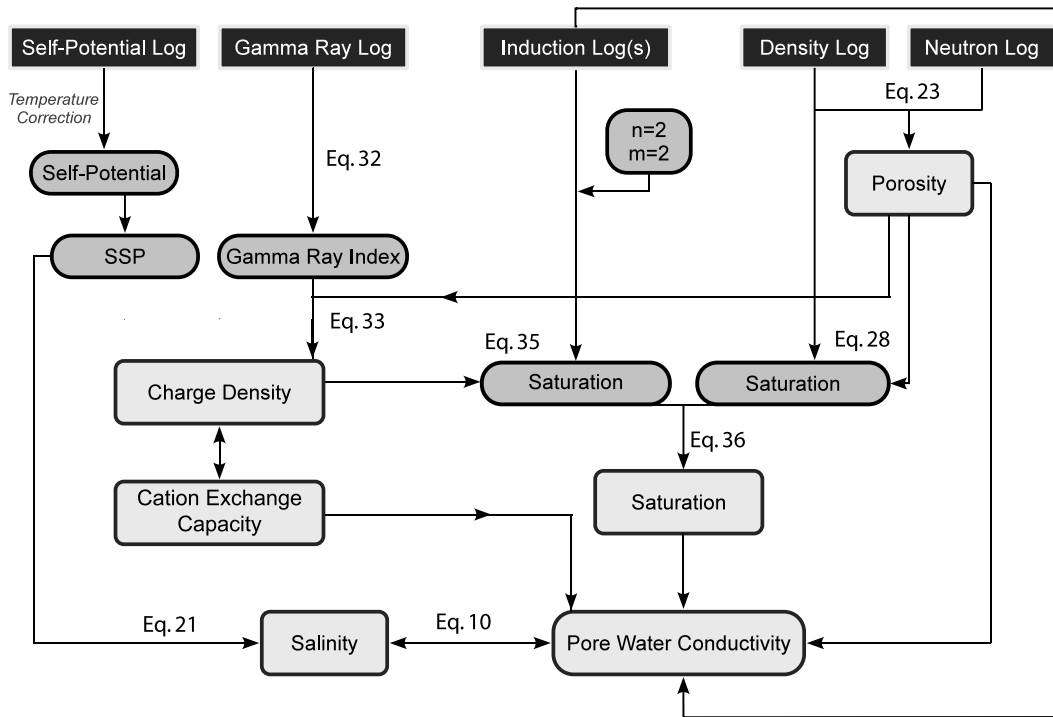


Figure 2. Workflow for determination of the first estimates of the six model parameters at each depth. These model parameters are the two Archie's exponents, the porosity, the saturation in water, the charge per unit pore volume or the CEC and the conductivity of the pore water (or alternatively the salinity).

with some prior knowledge. Bayesian analysis considers both the data vector \mathbf{d} and the model parameter vector \mathbf{m} of a model as random variables defined as probability distributions. All distributions are characterized by probability density functions (Mosegaard & Tarantola 1995). The objective of inverse modelling is to update the information on \mathbf{m} given the data \mathbf{d} and *a priori* knowledge of \mathbf{m} . Prior information can come from independent observations as well as petrophysical or theoretical relationships. The first estimate cannot be used directly as a prior as in principle the prior is not based on the data. We will discuss at the end of this section how the prior is chosen.

In a probabilistic framework, the inverse problem reduces to the maximization of the conditional probability, or 'likelihood', of the model response \mathbf{m} given the data vector \mathbf{d} and a petrophysical model M . We denote $P_0(\mathbf{m}|M)$ as the prior probability density or the best guess for parameters \mathbf{m} of model M and such a model generates the probability density of likelihood $P(\mathbf{d}|\mathbf{m}, M)$ corresponding to the data fit. The posterior probability density $\pi(\mathbf{m}|\mathbf{d})$ of the model parameters \mathbf{m} given the data \mathbf{d} is obtained by using Bayes formula,

$$\pi(\mathbf{m}|\mathbf{d}, M) = \frac{P(\mathbf{d}|\mathbf{m}, M)P_0(\mathbf{m}|M)}{P(\mathbf{d}|M)}, \quad (37)$$

where $P(\mathbf{d}|M)$, the evidence, is defined as,

$$P(\mathbf{d}|M) = \int P_0(\mathbf{m}|M)P(\mathbf{d}|\mathbf{m}, M)d\mathbf{m}. \quad (38)$$

In the following, we assume the petrophysical model M (described below) is certain and therefore we drop the term M . The posterior probability density $\pi(\mathbf{m}|\mathbf{d})$ of the model parameters \mathbf{m} given the data \mathbf{d} is written as,

$$\pi(\mathbf{m}|\mathbf{d}) \propto P(\mathbf{d}|\mathbf{m})P_0(\mathbf{m}). \quad (39)$$

The Bayesian solution of the inverse problem is the posterior probability distribution of material properties over the complete range of parameter values. An estimate of the unknown parameters can be computed as the expected value with respect to the posterior distribution (i.e. as the mean value) or as the maximum posterior value, which can be interpreted as the most likely value.

It is a widely accepted practice to define the likelihood function in terms of normally distributed range of values. The model response $g(\mathbf{m})$ is assumed to be Gaussian distributed,

$$P(\mathbf{d}|\mathbf{m}) = \frac{1}{[(2\pi)^N \det C_d]^{1/2}} \times \exp \left[-\frac{1}{2}(\mathbf{g}(\mathbf{m}) - \mathbf{d})^T C_d^{-1}(\mathbf{g}(\mathbf{m}) - \mathbf{d}) \right], \quad (40)$$

$$\mathbf{d} = (\mathbf{d}_v, \mathbf{d}_R, \mathbf{d}_{\text{rho}})^T, \quad (41)$$

where \mathbf{d} is an N -vector of the observed log data, C_d is the $(N \times N)$ -covariance matrix and $g(\mathbf{m})$ is the (non-linear) forward operator for the self-potential problem (note that while $P(\mathbf{d}|\mathbf{m})$ can be Gaussian, $P(\mathbf{m}|\mathbf{d})$ is Gaussian only if g is linear). The petrophysical model establishes a non-linear connection between the generation of downhole measurements and the random variations of model parameter values. The covariance matrix comprises the error associated with the measurement corresponding to each log, which are assumed to be uncorrelated and are to obey Gaussian statistics (i.e. they are defined by either normal or log normal distributions).

The prior distribution on the model parameters can be taken as Gaussian,

$$P_0(\mathbf{m}) = \frac{1}{[(2\pi)^M \det C_m]^{1/2}} \times \exp \left[-\frac{1}{2}(\mathbf{m} - \mathbf{m}_{\text{prior}})^T C_m^{-1}(\mathbf{m} - \mathbf{m}_{\text{prior}}) \right], \quad (42)$$

where $\mathbf{m}_{\text{prior}}$ is a vector of prior constraints, or expected values, of the petrophysical parameters in the subsurface and \mathbf{C}_m is the $(M \times M)$ -covariance matrix of the model, which incorporates the uncertainty (confidence) related to the imposed constraints. In the example presented below, we use a null-prior as the confidence interval for the model. In the classical Bayesian approach, the model parameter \mathbf{m} that best fits the geophysical observations \mathbf{d} , maximizes the posterior probability density $\pi(\mathbf{m}|\mathbf{d})$. The objective is to explore the posterior probability density $\pi(\mathbf{m}|\mathbf{d})$ through repeated stochastic realization of the model \mathbf{m} .

The MCMC family of algorithms is well-suited to Bayesian inference problems (Mosegaard & Tarantola 1995). MCMC algorithms consist of random walks where different posterior states (i.e. different-valued, random realization of a model vector) are visited through iterative solution of the forward operator. The choice of each subsequent state depends only on the value of the current state. After an initial period, during which the random walker moves toward regions of highest posterior probability, the chain returns a number of model vectors used to construct the posterior probability distribution $\pi(\mathbf{m}|\mathbf{d})$ of the model parameters. The vectors retained by the algorithm represent stochastic samples of the posterior probability density. If a sufficient number of samples of the posterior distribution have been obtained, characteristics of the posterior probability density, like the mean and the standard deviation, or the number of extrema, are easily determined. Memory mechanisms of MCMC algorithms (conditions requiring the chain to remain in regions of

high probability) are responsible for a greater efficiency of the algorithm by comparison to Monte Carlo methods. In this paper, we implemented a variant of the MCMC algorithm called the Adaptive Metropolis Algorithm (AMA, see Haario *et al.* 2001, 2004). More precisely, we use the algorithm described in Appendix A of Tamminen (2004). The starting value of the model parameters used to start the MCMC algorithm are those determined in Section 3.2 and Fig. 2.

The following is the petrophysical model used to perform the inversion:

$$\tilde{\rho} = (1 - \phi)\tilde{\rho}_s + \phi s_w \tilde{\rho}_w, \quad (43)$$

$$\frac{1}{\rho_f} = \phi^m \left[s_w^n e C_w (\beta_{(+)} + \beta_{(-)}) + \frac{(1-f)(1-\phi)\beta_{(+)}\tilde{\rho}_s I_{GR} \text{CEC}_{clay}}{s_w \phi} \right], \quad (44)$$

$$\nabla \cdot \left(\frac{1}{\rho} \nabla \psi \right) = \frac{k_b T}{e} \nabla \cdot \left[\frac{1}{\rho} (2T_{(+)} - 1) \nabla \ln \rho_w \right], \quad (45)$$

where the formation resistivity and the pore water resistivity are given by,

$$\rho = \begin{cases} \rho_m, & \text{for } 0 \leq r \leq R, \\ \rho_f & \text{for } r > R, \end{cases} \quad (46)$$

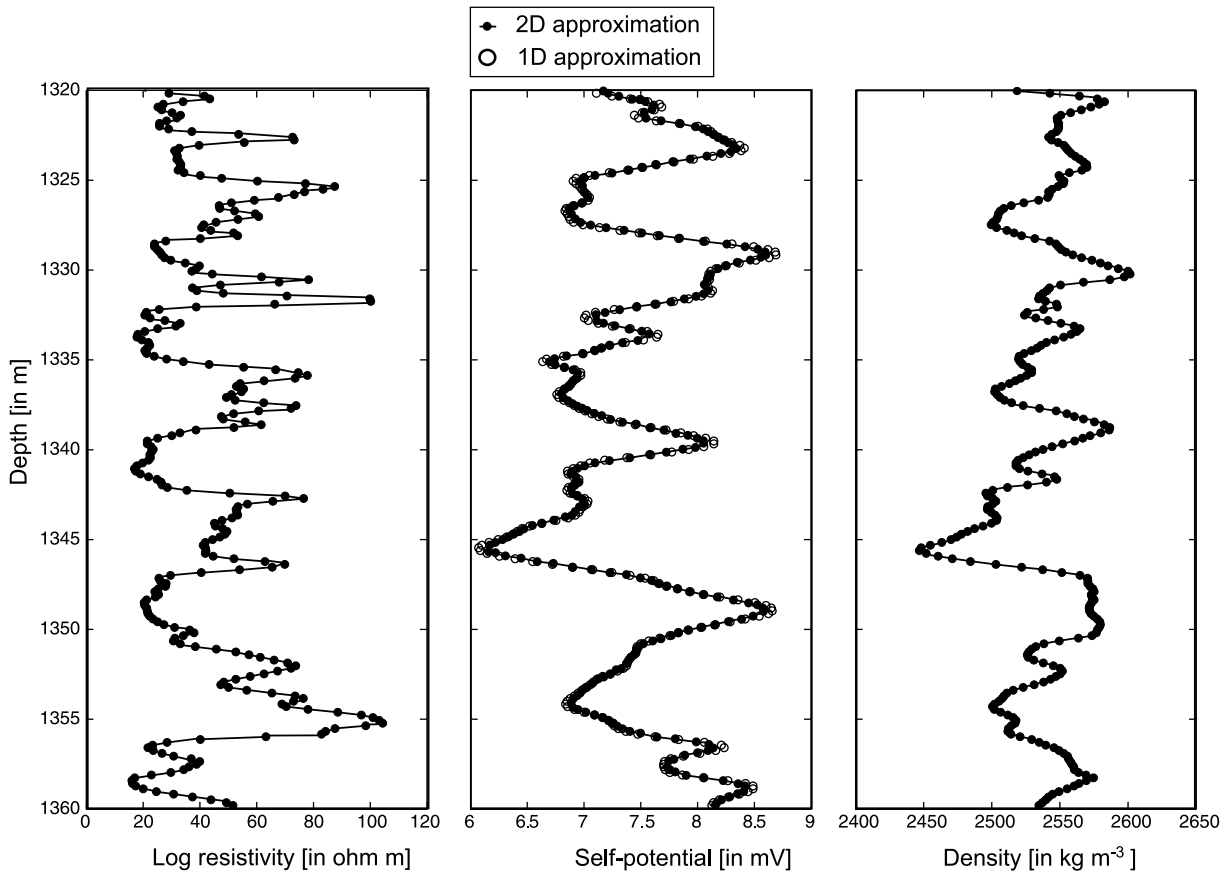


Figure 3. Borehole data used for the synthetic model. For the self-potential data, we compare the 2-D axisymmetric forward model response (plotted as black circles) to that of the 1-D axisymmetric forward model response computed at each depth (plotted as open circles). The similar response computed with the 1-D and 2-D axisymmetric models justifies the assumption that the vertical component of the electric field can be neglected in the analysis of the self-potential data when the salinity of the formation is constant.

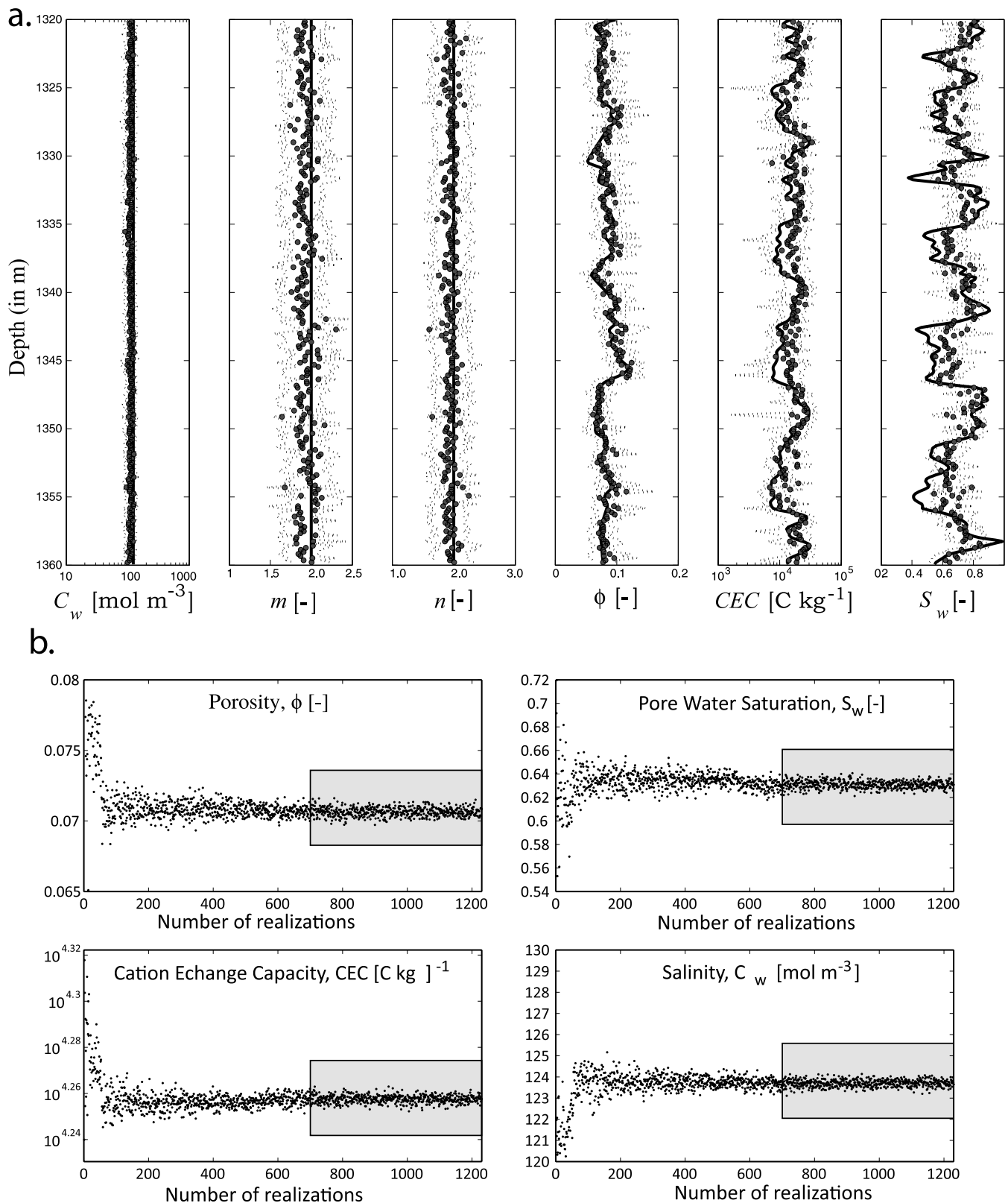


Figure 4. Results of the inversion of the six model parameters. (a) Inverted model parameters (plain circles) resulting from the 1-D axisymmetric inversion are plotted against the true model parameters used to generate the synthetic data set (the solid lines). The mean (grey circles) and standard deviation (the small black dots) of the posterior model distributions are shown for each depth. (b) Example of stochastic realizations of porosity, water saturation, cation exchange capacity and salinity values sampled during the inversion at a single depth. The distribution of parameter values approaches a constant mean and standard deviation, showing the distribution has converged. The posterior probability density of the model parameters is defined from the windowed interval.

$$\rho_w = \begin{cases} \rho_{mf}, & \text{for } 0 \leq r \leq R, \\ \rho_w = \frac{1}{eC_w(\beta_{(+)}+\beta_{(-)})} & \text{for } r > R, \end{cases} \quad (47)$$

respectively and the macroscopic Hittorf number is defined by,

$$T_{(+)} = \begin{cases} t_{(+)}, & \text{for } 0 \leq r \leq R, \\ \frac{s_w t_{(+)} \phi e C_w (\beta_{(+)} + \beta_{(-)}) + (1-f)(1-\phi) \beta_{(+)} \bar{\rho}_S I_{GR}^{CEC_{clay}}}{s_w e C_w (\beta_{(+)} + \beta_{(-)}) \phi + (1-f)(1-\phi) \beta_{(+)} \bar{\rho}_S I_{GR}^{CEC_{clay}}} & \text{for } r > R. \end{cases} \quad (48)$$

In addition, we also use eq. (32) to perform the inversion of borehole data. Eq. (48) is obtained from Eqs (6) to (10) and eq. (33). In these equations, R is the borehole radius determined from the caliper log, ρ_f is the resistivity of the formation, ρ_m is the resistivity of the mud and ρ_{mf} is the resistivity of the mud filtrate. The fact that eq. (45) is solved in 2-D (i.e. we solve the radial self-potential problem at each depth z), will be discussed in the next section. These equations are also computed at the *in situ* temperature using eq. (13).

Finally, we revisit the need to select a common reference for the data and the model. One possibility is to take the voltage defined by the median of the sand and shale baselines as the references. This choice is discussed in Appendix A. In the synthetic case presented in the next section, we will select the reference in a different way. The method employed for the determination of the reference is non-unique; as long as all the calculations are made consistently a choice of a reference voltage for the data is valid.

The starting model established in Section 3.2 and Fig. 2 is in fact not a true prior, since it is derived in part from the data used

in the inversion. However, the model probability density functions are ‘whitened’ significantly to allow proper sampling of the parameter space. The standard deviations of the model parameters are in fact significantly augmented (by a factor 2) for sufficient posterior sampling.

4 SYNTHETIC CASE

To test both the accuracy of the simplified model (1-D axisymmetric model) with respect to the general model (2-D axisymmetric model) and the efficacy of the inversion algorithm, a synthetic data set was generated. This synthetic model describes the self-potential response to a source of current derived from the electrodiffusion of ions between a layered sedimentary sequence and the boreholes as described by the governing field equations given above in Sections 2 and 3. The solution to the synthetic model represents the *a priori* response given the data and computed according to the formulation of the prior solution described above, excepting the assumption of using a constant connate water salinity of 110 Mol m^{-3} . The synthetic data set provides a platform from which to test the compatibility of the 1-D and 2-D axisymmetric self-potential models, as well as prove the convergence of the inversion algorithm.

The forward 1-D axisymmetric model requires the electrical response at a given depth to depend on a set of reference voltages at each depth. This reference corresponds to the measured voltages bounding a given depth along the borehole axis. The application of these reference points in the 2-D case compensates for

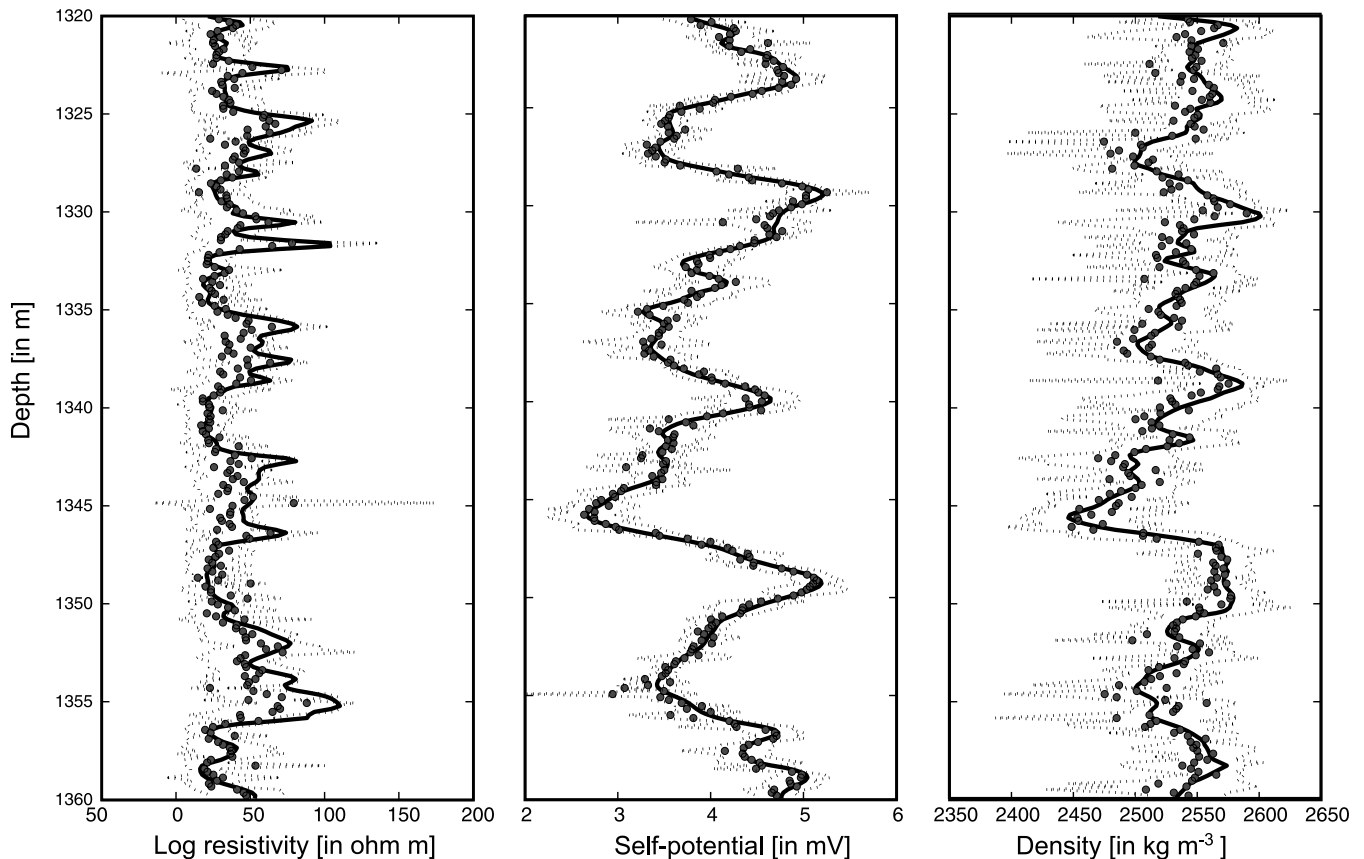


Figure 5. Posterior mean for the data at each depth resulting from the 1-D axisymmetric inversion (filled circles) are plotted against synthetic data generated by the 2-D axisymmetric model (the plain lines). The mean (filled grey circles) and standard deviation (black dots) of the posterior data distributions are shown for each depth. The solid lines represent the synthetic data.

Table 2. Mean and standard deviation of model parameters for the stratigraphic layers of the synthetic model determined according to the gamma-ray index. The mean and standard deviation (in parentheses) of the posterior distributions for each layer are tabulated. These results are in very good agreement with the true model parameter values (see solid lines in Fig. 4a): ϕ is the porosity, s_w is the saturation of the brine, C_w is the salinity of the pore water (in Mol m^{-3}), CEC is the cation exchange capacity (in C kg^{-1}) and m and n are the two Archie's exponents.

Layer	Lithology	ϕ	s_w	C_w	CEC ($\times 10^4$)	m	n
1	Shale	0.07 (0.019)	0.72 (0.090)	112 (20.6)	1.94 (0.87)	1.91 (0.24)	1.94 (0.28)
2	Sand	0.08 (0.020)	0.65 (0.098)	111 (22.0)	1.28 (0.72)	1.95 (0.22)	1.97 (0.29)
3	Shale	0.08 (0.019)	0.65 (0.088)	114 (20.5)	1.39 (0.54)	1.89 (0.24)	1.98 (0.29)
4	Sand	0.10 (0.018)	0.65 (0.097)	109 (22.9)	1.22 (0.59)	1.96 (0.26)	1.95 (0.27)
5	Shale	0.08 (0.020)	0.71 (0.106)	110 (21.9)	1.97 (0.91)	1.91 (0.24)	1.95 (0.27)
6	Sand	0.09 (0.019)	0.66 (0.102)	107 (20.7)	1.56 (0.88)	1.95 (0.24)	1.95 (0.28)
7	Shale	0.08 (0.022)	0.74 (0.096)	110 (21.6)	1.93 (0.88)	1.89 (0.25)	1.93 (0.26)
8	Sand	0.11 (0.031)	0.68 (0.122)	114 (25.3)	1.44 (0.65)	2.05 (0.24)	1.86 (0.22)
9	Shale	0.09 (0.017)	0.62 (0.108)	115 (21.0)	1.42 (0.69)	1.93 (0.26)	1.92 (0.28)
10	Sand	0.11 (0.022)	0.63 (0.098)	111 (20.7)	1.42 (0.84)	1.97 (0.26)	1.97 (0.28)
11	Shale	0.07 (0.015)	0.75 (0.075)	112 (21.3)	1.96 (0.87)	1.89 (0.24)	1.94 (0.26)
12	Sand	0.08 (0.018)	0.64 (0.100)	112 (21.3)	1.51 (0.78)	2.00 (0.23)	1.90 (0.26)
13	Shale	0.08 (0.012)	0.62 (0.073)	112 (20.1)	1.15 (0.38)	1.94 (0.24)	1.97 (0.25)
14	Sand	0.09 (0.023)	0.64 (0.091)	112 (20.7)	1.15 (0.57)	1.98 (0.27)	1.95 (0.26)
15	Shale	0.08 (0.020)	0.71 (0.107)	110 (21.4)	2.05 (0.11)	1.90 (0.23)	1.94 (0.29)

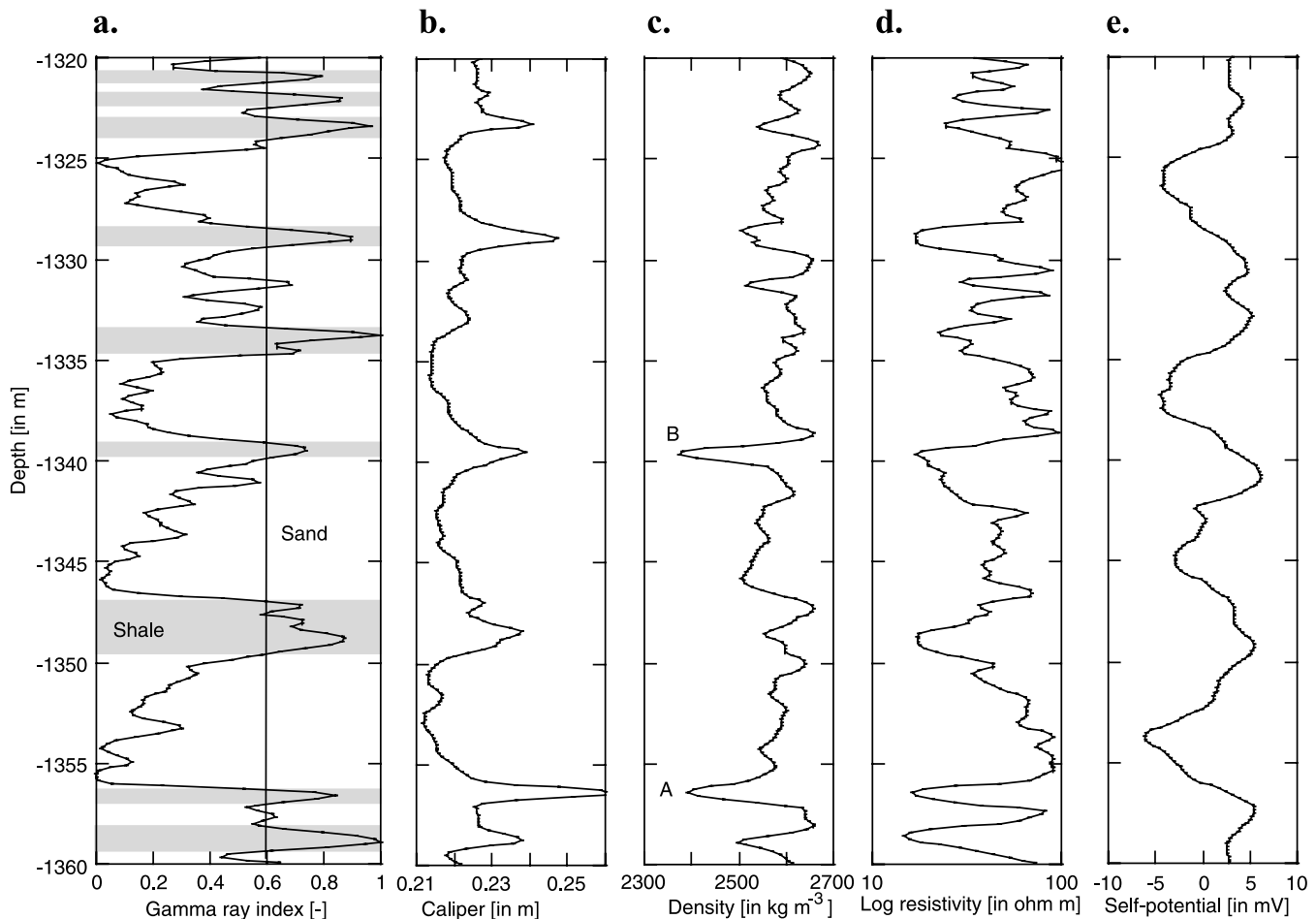


Figure 6. Borehole data collected in the Piceance Basin of western Colorado. An interval over a 40 m section of low porosity interbedded sand and shale layers was chosen for the analysis. (a) Gamma-ray index I_{GR} used as a lithology indicator to define sand (in white) and shale (in grey) layers. The vertical line corresponds to the critical value of the gamma-ray index used to distinguish between sand and shale layers. (b) Caliper log providing an estimate of the borehole radius. (c) Density log. Depth intervals A and B are examples of washouts corresponding to the erosion of the walls of the borehole at these depths. (d) Resistivity log (ILD). (e) Self-potential with a reference taken at the mid-values of the shale and sand baselines as explained in Appendix A.

any over or underestimation of the electric potential due to the absence of the vertical component of the electric field. Hence, the 2-D model computes the perturbation of electric potential from a reference defined by the data. A comparison of the forward response of the 1-D axisymmetric model to the synthetic is shown in Fig. 3. Since the synthetic apparent resistivity and bulk density obey linear relationships, the response of both models is identical to the true, prior values and is not shown here. The synthetic self-potential responses of the 2-D and 3-D numerical models are well correlated, verifying the 2-D assumption in the case where the salinity of the formation water is constant. The validity of the 2-D assumption simplifies the physical problem, improves computational cost and enables the iterative application of the model to a data set of arbitrary size. Note however this assumption is only valid as long as there is no sharp change in pore water salinity, because such sharp changes would generate vertical components in the self-potential field measured in the borehole, which may invalidate the use of the 2-D numerical approach. In this case, if the 2-D numerical modelling and inversion starts to exhibit drastic change in the vertical distribution of the formation salinity, it is better to use the 3-D numerical model, which accounts for such vertical contributions.

The synthetic data was also used to test the accuracy of the inversion algorithm. Since the true model parameter vector is known for the synthetic, it can be used to validate the posterior distributions of the model parameters output by the inversion. Therefore, we can test the accuracy of the convergence of the inversion as-

suming that the model is an exact solution to the physical problem. A direct comparison of the mean posterior parameter values to the prior shows good correlation (see Fig. 4), validating the inversion algorithm. A comparison between the posterior values of the data and the true data values is shown in Fig. 5, illustrating the high quality of the forward model as a proxy for reproducing the data.

We also looked at the posterior distributions defined by collections of (separately) inverted depths, which correspond to sand and shale layers, as defined according to the gamma-ray index applied in the formulation of the synthetic. The results of the 2-D axisymmetric inversion are classified and grouped with adjoining depths according to a criteria based on the gamma-ray index. Shales are grouped within depth intervals corresponding to a gamma-ray index greater than 0.5, whereas sands are defined by intervals corresponding to gamma-ray indices less than 0.5. The results of this comparison are reported in Table 2, indentifying 15 layers in the synthetic data. For each of these layers, we compute the average values of the posterior mean (inverted at each depth) and associated variance. These values are very close to the true values (e.g. $m = n = 2$ in the synthetic data set and the salinity of the formation is equal to 110 Mol m^{-3}). These results prove the good convergence of our inversion algorithm. The mean and variance of these composite distributions are a generalized measure of the material properties for each layer in the synthetic stratigraphic sequence and provide statistical methodology for the evaluation of stratigraphic relationships based on lithological criteria.

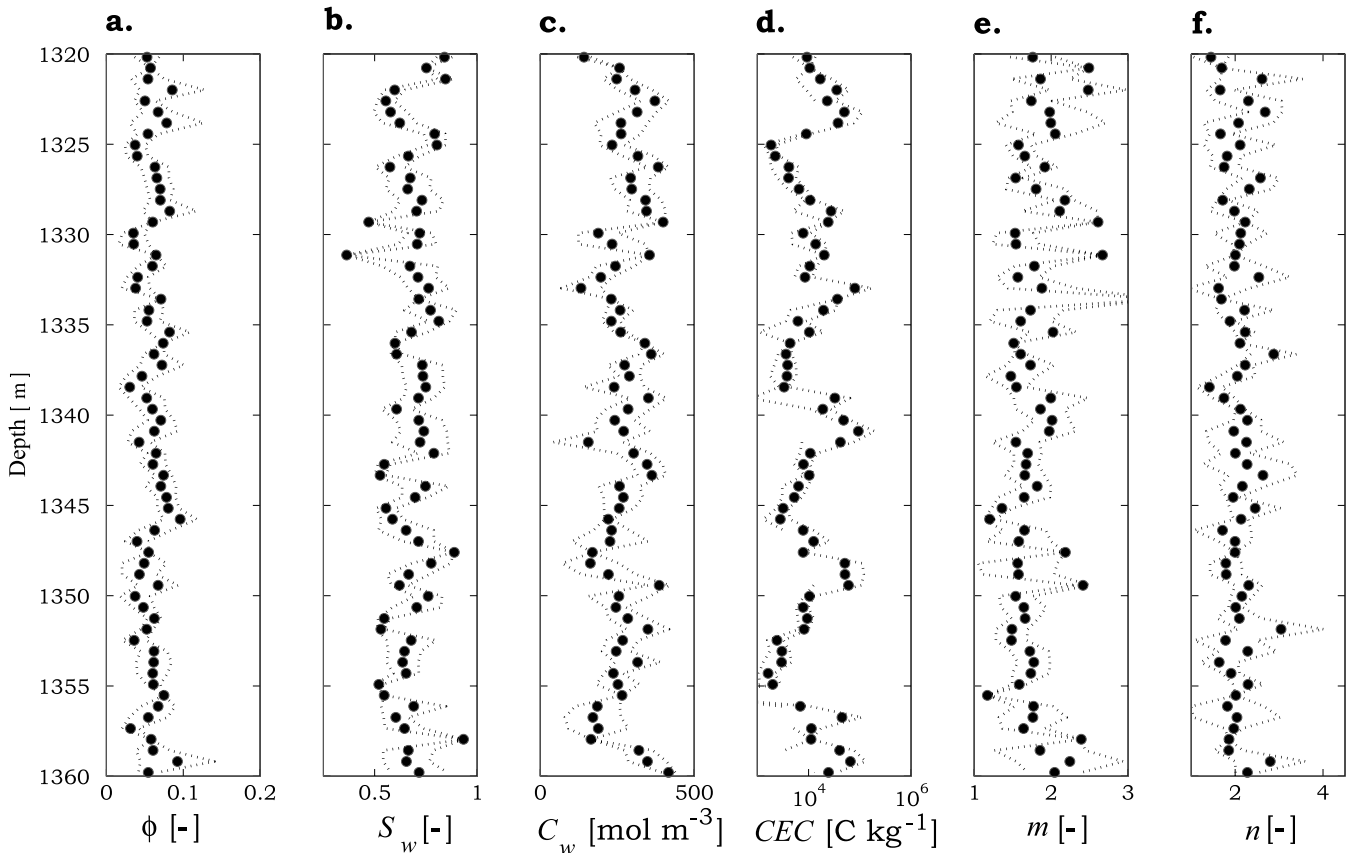


Figure 7. Posterior probability distribution of reservoir properties showed as the mean and the confidence interval at each depth. (a) Porosity ϕ . (b) Water saturation s_w . (c) Salinity C_w . (d) Cation exchange capacity, CEC. For comparison, the CEC of illite is $2 \times 10^4 \text{ C kg}^{-1}$. (e) First Archie exponent m (cementation exponent). (f) Second Archie exponent n (saturation exponent).

5 APPLICATION TO REAL DATA

The Piceance Basin in western Colorado is currently an area of interest for gas production in low permeability reservoirs. The stratigraphic section known as the Mesaverde Group comprising both fluvial and marine regression sequences of interstratified sandstone and shale layers overlying extensive coal formations and capped by a thin laterally continuous shale formation, is the site of a large, basin-centred gas accumulation (Cumella & Ostby 2003; Cumella & Scheevel 2008). We chose a 40 m section of a well exhibiting data characteristic of the interval bounding continuous top gas to test our model. The following borehole measurements are available for the analysis: caliper, gamma-ray, resistivity and density, neutron and temperature logs. They are used to construct a multilayer model geometry and define parameter values within the model space. Although regions within the model are indicated to represent sandstone and shale layers (see the white and grey areas in Fig. 6a), the model is, in essence, discretized vertically by the sampling interval of the data.

5.1 Data set characteristics and material properties

Using the model described in Section 2 and the stochastic approach outlined in Section 3, a multiparameter joint inversion of self-potential, bulk density and resistivity data was performed. The segment of the data set chosen for this analysis is characterized by a well-defined sequence of sand and shale layers (Fig. 6). The interval is also characterized by low porosity (less than 0.2 according to neu-

tron and density logs), minimal invasion, volumetrically negligible amount of K-feldspar mineral in sand and relatively thin interbedding within the formations. The gamma-ray, resistivity and neutron curves clearly delineate the interstratified sandstone shale sequence, whereas the relatively low range of the photo-electric density curve indicates minimal calcification of the sand intervals. For the induction curves as well as the shallow laterolog, all track are very closely with one another. This indicates that the depth of invasion of the drilling mud in the formation is minimal. Areas of large separation in these curves also correlate to significantly high caliper and anomalously low density readings in shales, which are indicators of washout.

The value for the conductivity of the mud is 0.5 S m^{-1} and the conductivity of the mud filtrate is 0.667 S m^{-1} at 25°C . The conductivity of the connate water is assumed to be on the order of $2\text{--}6 \text{ S m}^{-1}$, a range of values commonly used for formation water in the Piceance Basin. The temperature gradient is constant throughout the section and equal to $0.05^\circ\text{C m}^{-1}$.

5.2 Results of the joint inversion

The AMA algorithm is used to invert five model parameters: the salinity (C_w), the cementation exponent (m), the saturation exponent (n), the water saturation (S_w), the porosity (ϕ) and the cation exchange capacity (CEC). We used the self-potential, deep induction and density well logs in the inversion. In addition to the constraints discussed in Section 3, we use the following bounds for the model parameters: $C_w \in [1, 100] \text{ Mol m}^{-3}$, $m \in [1; 5]$, $n \in [1; 5]$ and

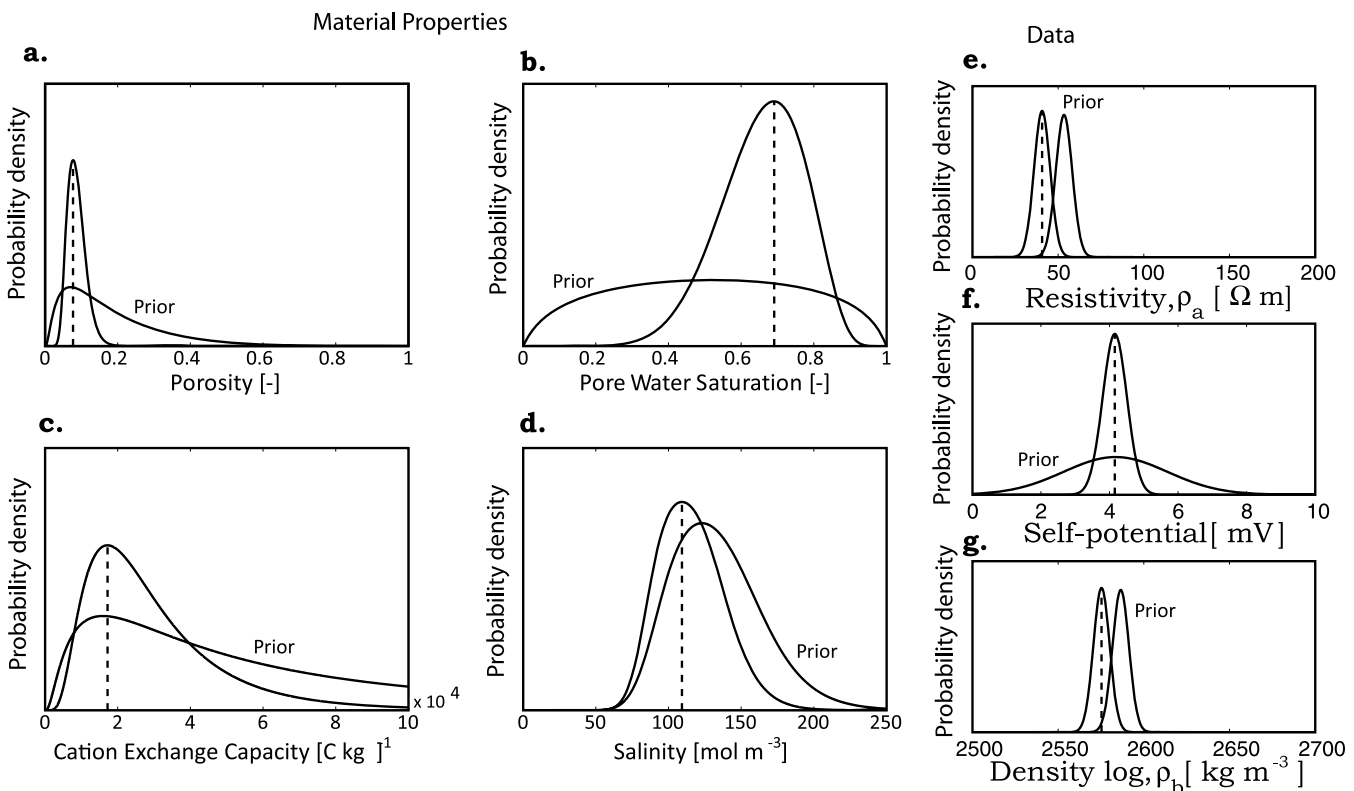


Figure 8. Comparison between the prior and posterior probability density functions for the material properties and data assuming Gaussian distributions for the log or the log of the model parameters. (a) Porosity (dimensionless), (b) Connate (pore) water saturation (dimensionless). (c) Cation exchange capacity of the clay fraction (in C kg^{-1}). (d) Concentration of dissolved salts (salinity) in formation waters (in Mol m^{-3}). (d, e, f) Downhole measurements (data) prior and posterior probability distributions at a given depth.

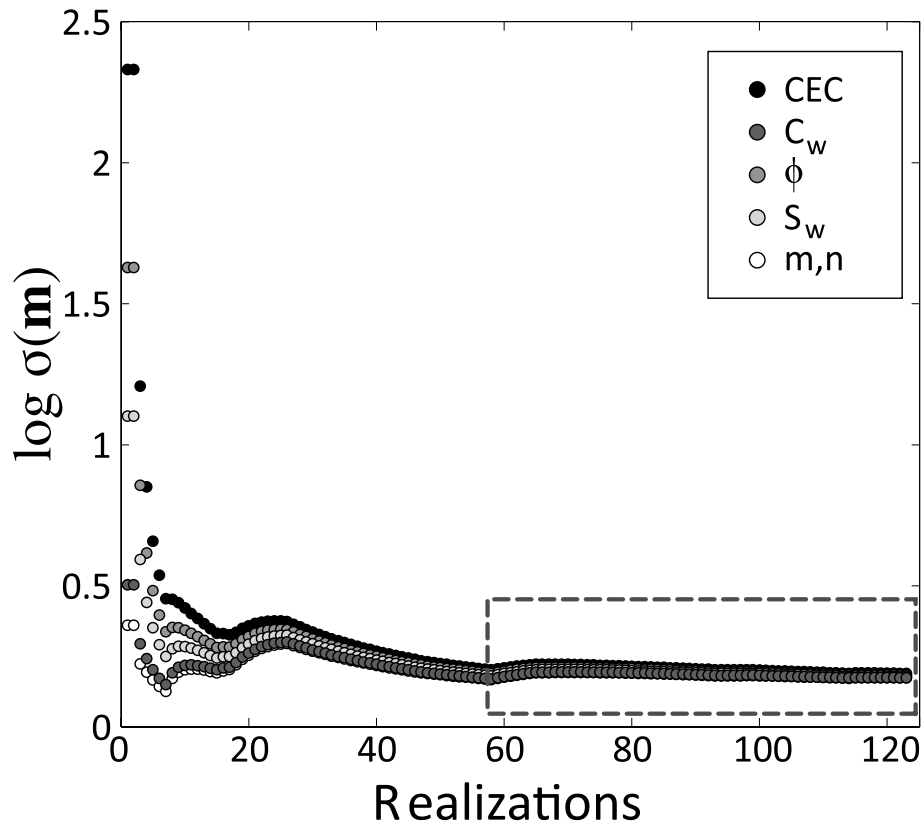


Figure 9. Evolution of the standard deviations of the model parameters as a function of the number of realizations using the AMA algorithm at a given depth. This computation is performed at each depth to determine the number of realizations required for the algorithm to converge. In this case, the algorithm converges after 50–60 realizations and the additional realizations (inside the dashed box) are used to compute the posterior probability density on each model parameter at each depth.

$CEC \in [1-10^5] \text{ C kg}^{-1}$ (the porosity and the saturation are comprised between 0 and 1).

The data vector, \mathbf{d} , is populated with log curves for the interval discussed in Section 5.1. The misfit function is solved iteratively, comparing the model response, $g(\mathbf{m})$, to the observed self-potential, resistivity, density and gamma-ray logs. This is equivalent to the maximization of the posterior probability density $\pi(\mathbf{m}|\mathbf{d})$. The initial model vector is populated by reasonable prior values as described in Section 3.2. Prior constraints on the model parameter vector, \mathbf{m} , are given using the bounds discussed above on the model parameters or on the variables used to estimate the model parameters.

The inversion yields the model parameters \mathbf{m}_{post} at each depth. These results are consistent with the geology of the Piceance Basin (Fig. 7). The range of values of the parameters of interest are the following: $C_w \in [18, 541] \text{ Mol m}^{-3}$, $m \in [1, 3.02]$, $n \in [1, 3.57]$, $S_w \in [0.05, 0.99]$ (volume fraction), $\phi \in [0.03, 0.14]$ (volume fraction) and $CEC \in [500, 3.4 \times 10^4] \text{ C kg}^{-1}$. The prior and posterior probability density functions for the model parameters are illustrated for the inversion of a single depth in Figs 8(a)–(d). Prior and posterior probability densities on the data are shown in Figs 8(e)–(f) at a single depth. The probability density for the model parameters is computed for all the realizations made at each once the algorithm has converged as shown in Fig. 9.

The posterior model response exhibited a satisfactory fit to the data, which was within a mean and standard deviation of the posterior model variance of 21.4 and 6.45 Ohm m, 2.23 and 0.8 mV

and 41.12 and 11.34 kg m^{-3} for resistivity, self-potential and bulk density, respectively, over the entire section (Fig. 10). This degree of accuracy was achieved within a relatively low number of iterations (fewer than 100 per depth iterate), as the convergence criteria were met quickly using the AMA algorithm.

6 CONCLUDING STATEMENTS

A mechanistic model has been developed to interpret the measurements of the self-potential in boreholes. The model accounts for both a diffusion potential due to the difference in the activity of the charge carriers between the formation water and the drilling mud and a streaming potential contribution due to the difference in fluid pressure between the formation and the borehole. Self-potential data can be inverted with additional borehole data (in the present case, resistivity, density, neutron porosity and gamma-ray logs) to retrieve probability densities of some key petrophysical properties such as the porosity, the saturation of the water phase, the two Archie's exponents (the cementation and the saturation exponents) and a charge per unit volume. To achieve this goal, we have used a highly adaptable and efficient MCMC approach, which provides posterior probability densities for both the model parameters and the data used in the inversion. Further development of this method will lead to a basin-wide analysis or shallow subsurface applications and the ability to invert for additional parameters, such as *in situ* permeability, as some of the parameters inverted in this work (especially

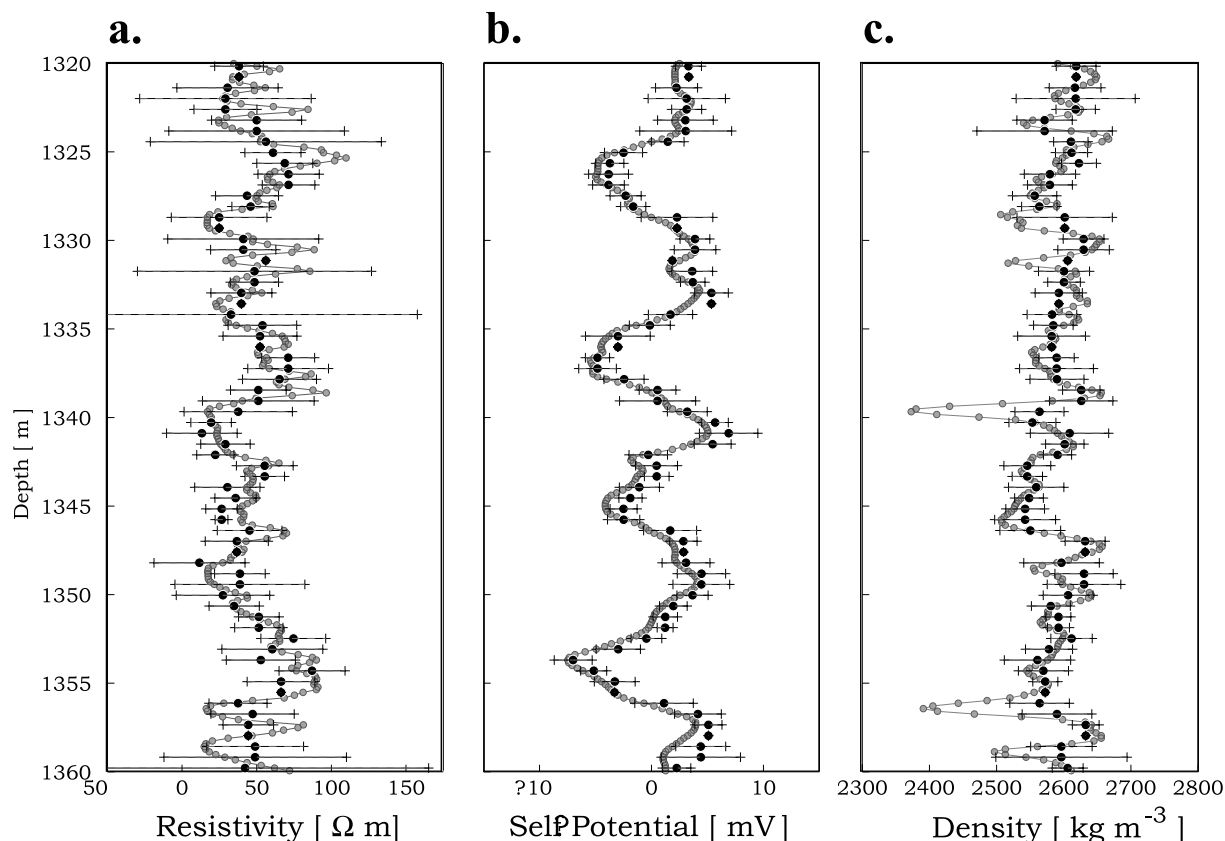


Figure 10. Data Misfit. Inversion results showing the model of highest likelihood with corresponding error bars determined by the posterior probability distribution. (a) Resistivity. (b) Self-potential. (c) Density log. The *in situ* measurements are shown in grey-filled circles. The inverted data are shown with the black-filled circles. The error bars correspond to twice the standard deviations determined from the posterior probability density function on the data at each depth.

the charge per unit pore volume) are very sensitive to permeability (see Jardani *et al.* 2009).

ACKNOWLEDGMENTS

We thank Terry Young for his support at CSM, Mary Carr at CSM for providing access to tools for petrophysical analysis and Steve Sunnenberg for his assistance. The MS thesis of Bill Woodruff is funded through RPSEA Program at Mines. We thank two anonymous referees for their very helpful comments and the Associate Editor, Dr. Jun Korenaga.

REFERENCES

- Antelman, M.S., 1989. *The Encyclopedia of Chemical Electrode Potentials*, Plenum Press, New York.
- Archie, G.E., 1942. The electrical resistivity log as an aid in determining some reservoir characteristics, *Trans. Am. Inst. Min. Metall. Pet. Eng.*, **146**, 54–62.
- Arora, T., Revil, A., Linde, N. & Castermant, J., 2007. Non-intrusive determination of the redox potential of contaminant plumes using the self-potential method, *J. Contaminant Hydrol.*, **92**(3–4), 274–292.
- Bolève, A., Crespy, A., Revil, A., Janod, F. & Mattiuzzo, J.L., 2007. Streaming potentials of granular media: influence of the Dukhin and Reynolds numbers, *J. geophys. Res.*, **112**, B08204, doi:10.1029/2006JB004673.
- Castermant, J., Mendonça, C.A., Revil, A., Trolard, F., Bourrié, G. & Linde, N., 2008. Redox potential distribution inferred from self-potential measurements during the corrosion of a burden metallic body, *Geophys. Prospect.*, **56**, 269–282, doi:10.1111/j.1365-2478.2007.00675.x.
- Clennel Palmer, A. & King, R.A., 2004. *Subsea Pipeline Engineering*, p. 570, PennWell Books, Tulsa, OK.
- Cumella, S.P. & Ostby, D.B., 2003. Geology of the basin-centered gas accumulation, Piceance Basin, Colorado, in *Piceance Basin 2003 Guidebook*, pp. 171–193, eds Peterson, K.M., Olson, T.M. & Anderson, D.S., Rocky Mountain Association of Geologists, Denver, CO.
- Cumella, S.P. & Scheevel, J., 2008. The influence of stratigraphy and rock mechanics on Mesaverde gas distribution, Piceance Basin, Colorado, in *Understanding, Exploring and Developing Tight-Gas Sands*, Vol. 3, pp. 137–155, eds Cumella, S.P., Shanley, K.W. & Camp, W.K., AAPG Hedberg Series, Vail, CO.
- Doll, H.G., 1949. *The S.P. Log: Theoretical Analysis and Principles of Interpretation*, Vol. 179, pp. 146–185, Transactions of American Institute of Mining, Metallurgical, and Petroleum Engineers, New York.
- Ellis, D.V. & Singer, J.M., 2007. *Well Logging for Earth Scientists*, 2nd edn, p. 692, Springer, Dordrecht.
- Ghorbani, A., Camerlynck, C., Florsch, N., Cosenza, P., Tabbagh, A. & Revil, A., 2007. Bayesian inference of the Cole-Cole parameters from time and frequency-domain induced polarization, *Geophys. Prospect.*, **55**(4), 589–605, doi:10.1111/j.1365-2478.2007.00627.x.
- Gelius, L.J. & Wang, Z., 2008. Modeling production changes in conductivity for a siliclastic reservoir: a differential effective medium approach, *Geophys. Prospect.*, **56**(5), 677–691.
- Haario, H., Saksman, E. & Tamminen, J., 2001. An adaptive Metropolis algorithm, *Bernoulli*, **7**, 223–242.
- Haario, H., Laine, M., Lehtinen, M., Saksman, E. & Tamminen, J., 2004. MCMC methods for high dimensional inversion in remote sensing, *J. R. Stat. Soc., Ser. B*, **66**, 591–607.

- Hearst, J.R. & Nelson, P., 1985. *Well Logging for Physical Properties*, McGraw Hill, New York.
- Hötzl, H. & Merkle, G.-P., 1989. Self-potential measurements to determine preferred waterflow in fractured rocks in Lecture Notes in Earth Sciences, in *Detection of Subsurface Flow Phenomena*, Vol. 27, pp. 147–156, Springer-Berlin, Heidelberg.
- Hunt, C.W. & Worthington, M.H., 2000. Borehole electrokinetic responses in fracture dominated hydraulically conductive zones, *Geophys. Res. Lett.*, **27**(9), 1315–1318.
- Jardani, A., Revil, A., Santos, F., Fauchard, C. & Dupont, J.P., 2007. Detection of preferential infiltration pathways in sinkholes using joint inversion of self-potential and EM-34 conductivity data, *Geophys. Prospect.*, **55**, 1–11, doi:10.1111/j.1365-2478.2007.00638.x.
- Jardani, A., Revil, A., Bolève, A. & Dupont, J.P., 2008. 3D inversion of self-potential data used to constrain the pattern of ground water flow in geothermal fields, *J. geophys. Res.*, **113**, B09204, doi:10.1029/2007JB005302.
- Jardani, A. *et al.*, 2009. Reconstruction of the water table from self potential data: a Bayesian approach, *Ground Water*, **47**(2), 213–227.
- Jougnot, D., Revil, A. & Leroy, P., 2009. Diffusion of ionic tracers in the Callovo-Oxfordian clay-rock using the Donnan equilibrium model and the electrical formation factor, *Geochim. Cosmochim. Acta*, **73**, 2712–2726.
- Leroy, P., Revil, A., Kemna, A., Cosenza, P. & Gorbani, A., 2008. Spectral induced polarization of water-saturated packs of glass beads, *J. Colloid Interface Sci.*, **321**(1), 103–117.
- Leroy, P., Revil, A., Altmann, S. & Tournassat, C., 2007. Modeling the composition of the pore water in a clay-rock geological formation (Callovo-Oxfordian, France), *Geochim. Cosmochim. Acta*, **71**(5), 1087–1097, doi:10.1016/j.gca.2006.11.009.
- Linde, N. & Revil, A., 2007. Inverting residual self-potential data for redox potentials of contaminant plumes, *Geophys. Res. Lett.*, **34**, L14302, doi:10.1029/2007GL030084.
- Linde, N., Jougnot, D., Revil, A., Matthäi, S.K., Arora, T., Renard, D. & Doussan, C., 2007. Streaming current generation in two-phase flow conditions, *Geophys. Res. Lett.*, **34**(3), L03306, doi:10.1029/2006GL028878.
- Maineult, A., Bernabé, Y. & Ackerer, P., 2005. Detection of advected concentration and pH fronts from self-potential measurements, *J. geophys. Res.*, **110**(B11), B11205, doi:10.1029/2005JB003824.
- Maineult, A., Bernabé, Y. & Ackerer, P., 2006. Detection of advected, reacting redox fronts from self-potential measurements, *J. Contaminant Hydrol.*, **86**, 32–52.
- Mendonça, C.A., 2008. Forward and Inverse self-potential modeling in mineral exploration, *Geophysics*, **73**(1), F33–F43.
- Minsley, B., Sogade, J. & Morgan, F.D., 2007a. 3D source inversion of self-potential data, *J. geophys. Res.*, **112**, B02202, doi:10.1029/2006JB004262.
- Minsley, B., Sogade, J. & Morgan, F.D., 2007b. Three-dimensional self-potential inversion for subsurface DNAPL contaminant detection at the Savannah River Site, South Carolina, *Water Resour. Res.*, **43**, W04429, doi:10.1029/2005WR03996.
- Mojid, M.A. & Cho, H., 2008. Wetting solution and electrical double layer contributions to bulk electrical conductivity of sand-clay mixtures, *Vasozone J.*, **7**(3), 972–980.
- Mosegaard, K. & Tarantola, A., 1995. Monte Carlo sampling of solutions to inverse problems, *J. geophys. Res.*, **100**, 12 431–12 447.
- Pan, K.-J., Tan, Y.J. & Hu, H.L., 2009. Mathematical model and numerical method for spontaneous potential log in heterogeneous formations, *Appl. Math. Mech.*, **30**(2), 209–219.
- Petiau, G., 2000. Second generation of lead-lead chloride electrodes for geophysical applications, *Pure appl. Geophys.*, **157**, 357–382.
- Pezard, P.A., Gautier, S., Le Borgne, T., Legros, B. & Deltombe, J.-L., 2009. MuSET: a multiparameter and high precision sensor for downhole spontaneous electrical potential measurements, *C. R. Geosci.*, **341**(10–11), 795–975.
- Pirson, S.J., 1963. *Handbook of Well Log Analysis: For Oil and Gas Formation Evaluation*, Prentice-Hall, Inc., Englewood Cliffs, NJ.
- Rabaute, A., Revil, A. & Brosse, E., 2003. In situ mineralogy and permeability logs from downhole measurements. Application to a case study in clay-coated sandstone formations, *J. geophys. Res.*, **108**, 2414, doi:10.1029/2002JB002178.
- Revil, A., 1999. Ionic diffusivity, electrical conductivity, membrane and thermoelectric potentials in colloids and granular porous media: a unified model, *J. Colloid Interface Sci.*, **212**, 503–522.
- Revil, A., 2007. Thermodynamics of transport of ions and water in charged and deformable porous media, *J. Colloid Interface Sci.*, **307**(1), 254–264.
- Revil, A. & Leroy, P., 2001. Hydroelectric coupling in a clayey material, *Geophys. Res. Lett.*, **28**(8), 1643–1646.
- Revil, A. & Linde, N., 2006. Chemico-electromechanical coupling in microporous media, *J. Colloid Interface Sci.*, **302**, 682–694.
- Revil, A., Cathles, L.M., Losh, S. & Nunn, J.A., 1998. Electrical conductivity in shaly sands with geophysical applications, *J. geophys. Res.*, **103**(B10), 23 925–23 936.
- Revil, A., Linde, N., Cerepi, A., Jougnot, D., Matthäi, S. & Finsterle, S., 2007. Electrokinetic coupling in unsaturated porous media, *J. Colloid Interface Sci.*, **313**(1), 315–327, doi:10.1016/j.jcis.2007.03.037.
- Revil, A., Trolard, F., Bourrié, G., Castermant, J., Jardani, A. & Mendonça, C.A., 2009. Ionic contribution to the self-potential signals associated with a redox front, *J. Contaminant Hydrol.*, **109**, 27–39.
- Rieger, P.H., 1994. *Electrochemistry*, p. 483, Springer, Berlin.
- Salazar, J.M., Wang, G.L., Torres-Verdin, C. & Lee, H.J., 2008. Combined simulation and inversion of SP and resistivity logs for the estimation of connate-water resistivity and Archie's cementation exponent, *Geophysics*, **73**(3), E107–E114.
- Segesman, F., 1962. New SP correction charts, *Geophysics*, **27**(1), 815–828.
- Sill, W.R., 1983. Self-potential modelling from primary flows, *Geophysics*, **48**, 76–86.
- Stoll, J., Bigalke, J. & Grabner, E.W., 1995. Electrochemical modelling of self-potential anomalies Electrochemical modelling of self-potential anomalies, *Surv. Geophys.*, **16**(1), 107–120.
- Tabanou, J.R., Rouault, G.F. & Glowinski, R., 1987. SP deconvolution and quantitative interpretation in shaly sands, in *Proceedings of the Trans. SPWLA 28th Annual Logging Symposium*, Paper SS, London, 25pp.
- Taherian, M.R., Habashy, T.M., Schroeder, R.J., Mariani, D.R. & Chen, M.-Y., 1995. Laboratory study of the spontaneous potential–experimental and modeling results, *The Log Anal.*, **36**(5), 34–48.
- Tamminen, J., 2004. Validation of nonlinear inverse algorithms with Markov chain Monte Carlo method, *J. geophys. Res.*, **109**, D19303, doi:10.1029/2004JD004927.
- Ugbo, J.O., Kelly, B.F.J. & Ward, C.R., 2009. Estimation of an equivalent shaliness parameter using resistivity and spectroscopy logs: a total expansive clay approach, *J. Pet. Geol.*, **32**(4), 383–406.
- Waxman, M.H. & Smits, L.J.M., 1968. Electrical conductivities in oil bearing shaly sands, *J. pet. Eng. J.*, **8**, 107–122.
- Winter, H., Stoll, J. & Aulbach, E., 1991. *The New Electrical Potential Logging Tool, Scientific Drilling*, Vol. 2, pp. 147–159, Springer-Verlag, Heidelberg.
- Worthington, A.E. & Meldau, R.F., 1958. Departure curves for the self-potential log, *J. pet. Technol.*, **10**, 11–16.
- Zhang, G.J. & Wang, G.L., 1997. Application of vector potential theory to spontaneous potential calculation, *Radio Sci.*, **32**, 899–905.
- Zhang, G.J. & Wang, G.L., 1999. A new approach to SP-vector potential approach, *IEEE Trans. Geosci. Remote Sens.*, **37**, 2092–2098.

APPENDIX A: THE REFERENCE POTENTIAL

The choice of a reference voltage for self-potential measurements is quite arbitrary. One possible choice, for instance, is to select the reference as the median of the sand and shale baselines given by eq. (19) and (20), respectively. Therefore, we use the following potential to retrieve to the sand and shale baselines:

$$\Delta\psi = \frac{k_b T}{e} t_{(+)} \ln \left(\frac{\rho_m}{\rho_w} \right), \quad (\text{A1})$$

which corresponds to half the sum of the clean sand and pure shale baselines. With this choice of reference potential, the sand and shale baselines are now given by,

$$\Delta\psi_{sd} = \frac{k_b T}{e} (t_{(+)} - 1) \ln \left(\frac{\rho_m}{\rho_w} \right), \quad (\text{A2})$$

$$\Delta\psi_{sh} = -\Delta\psi_{sd}, \quad (\text{A3})$$

respectively. To remain consistent within the data set, the potential given by eq. (A1) must be retrieved for all computed potentials. For

instance eq. (18) of the main text becomes,

$$\Delta\psi = -\frac{k_b T}{e} (2T_{(+)} - t_{(+)} - 1) \ln \left(\frac{\sigma_m}{\sigma_w} \right). \quad (\text{A4})$$

If we use a finite element code to solve eq. (14), the following source term is used in lieu of eq. (13):

$$\mathbf{j}_s = -\frac{k_b T}{e} \sigma_0 (2T_{(+)} - t_{(+)} - 1) \nabla \ln \sigma_w. \quad (\text{A5})$$

Alternatively, if eq. (13) is used, the potential given by eq. (A1) must be removed from the computed potential field to remain consistent with the chosen reference voltage.